



School of Chemistry

Beta - Enhanced Thermionic Emission Studies of Semiconducting Diamond

Heather Bolton

**This thesis is submitted in partial fulfilment of the requirements for the Honours
Degree of MSci (Bsc) at the University of Bristol**

Supervisor: Neil Fox

Second Assessor: Paul May

Physical and Theoretical Group

Table of Contents

1	Glossary of terms	4
2	Abstract	5
3	Introduction	6
3.1	<i>Thermionic Emission</i>	6
3.1.1	Photoelectric effect	6
3.1.2	Thermionic Emission & TECs.....	6
3.1.3	TEC Applications.....	9
3.1.4	TEC Efficiency	9
3.2	<i>Diamond</i>	10
3.2.1	Properties	10
3.2.2	Synthesis	13
3.2.3	Diamond film - grain size	17
3.2.4	Further applications.....	19
3.2.5	Diamond films – doping	19
3.2.6	H termination	22
3.2.7	Schottky Junction.....	25
3.2.8	Characterisation	26
3.3	<i>Beta enhancement</i>	27
3.3.1	Radioisotopes... ..	27
3.3.2	Previous Studies.....	28
3.3.3	The aims of this study.....	29
4	Experimental Procedures	29
4.1	<i>Overview</i>	29
4.2	<i>Sample Preparation</i>	30
4.2.1	Diamond... ..	30
4.2.2	Molybdenum.....	34
4.2.3	H-Termination.....	36
4.2.4	Deuterium Termination.....	37
4.3	<i>Measuring emission</i>	37
4.3.1	Experiment Set-up.....	37
4.3.2	Emitter Set-up	38
5	Methodology	39
5.1	<i>Experimental Runs</i>	39
6	Results / Discussion	40
6.1	<i>Sample Preparation</i>	40

6.1.1	Diamond MPCVD 1.....	40
6.1.2	Laser cutting.....	41
6.1.3	Final Growth	42
6.1.4	H Termination.....	43
6.2	<i>Morphology Investigations</i>	44
6.2.1	HMo1	44
6.3	<i>Thermionic Emission</i>	46
6.3.1	Thermionic experiments	46
6.3.2	Beta Enhanced Thermionic Emission (BETE)	46
6.3.3	Mechanism of BETE.....	47
6.3.4	Threshold temperature	50
6.3.5	Further observations.....	52
6.4	<i>Deuterium Terminations</i>	53
7	Future Outlooks	55
8	Conclusion	56
9	Acknowledgements	57
10	References	57

1 Glossary of terms

Acronym	Meaning
TEC	Thermionic Energy Conversion
HPHT	High-Pressure High-Temperature
CVD	Chemical Vapour Deposition
HFCVD	Hot Filament CVD
DC CVD	Direct Current CVD
MPCVD	Electron plasma CVD
NCD	Nanocrystalline Diamond
UNCD	Ultra-nanocrystalline Diamond
HTND	Hydrogen Terminated Nanocrystalline Diamond
DOS	Density of States
SAW	Surface Acoustic Waves
VB	Valence Band
CB	Conduction Band
NEA	Negative Electron Affinity
RTG	Radioisotope Thermoelectric Generators
SEE	Secondary Electron Emission
RIC	Radiation Induced Conductivity
SEM	Scanning Electron Microscope
BETE	Beta enhanced thermionic emission

2 Abstract

Thermionic energy converters (TECs) directly convert solar energy into electrical energy and make for a promising renewable energy source. This report looks at incorporating beta electrons into a diamond TEC in order to enhance thermionic current output.

Two 10×10 mm samples were prepared as the emitting materials; diamond and molybdenum. A layer of high-quality nitrogen doped diamond was grown on both samples. The 'high-quality' and 'nitrogen' doping helps enhance the conductivity of diamond facilitating the motion of electrons from the surface. The samples were also surface terminated with hydrogen. This provides a negative electron affinity and further promotes the emission of electrons. During the decay of ^{63}Ni , beta electrons of average energy 17.3 keV are produced. ^{63}Ni (2.6 MBq) was used as the beta source in this report and was placed underneath the samples. In order for the beta electrons to reach the high-quality nitrogen doped, diamond two 3×3.5 mm hole arrays were milled through the samples in opposing corners.

Samples were heated to 600°C and the thermionic current measured for each experimental run. Upon incorporation of ^{63}Ni there was a 65% enhancement in emission from the diamond sample. The hydrogen desorbs from the surface at these temperatures and samples were re-terminated before each run. The main mechanisms creating the enhanced emission are believed to be either i) the beta electrons causing an increase in conductivity by production of electron hole pairs or ii) the beta electrons altering the skew of electrons in high energy states, thereby promoting their emission. Further research is needed to examine beta enhancement for the more conductive molybdenum sample which will perhaps shed more light on whether the mechanism is from heightened conductivity or non-conductive means.

Deuterium surface termination was also examined for both samples. No conclusive statements could be drawn on its effect on thermionic emission. However, deuterium did not need re-termination when the sample was heated to 600°C as deuterium appeared to desorb at higher temperatures. More research would be advantageous in order to determine whether emission is reduced using deuterium instead of hydrogen and whether the effects of deuterium alter between the molybdenum and the diamond sample.

3 Introduction

3.1 Thermionic Emission

3.1.1 Photoelectric effect

The emission of electrons to induce a current was first noted in 1887 when Hertz discovered an electric current occurring across two electrodes irradiated with electromagnetic radiation. The current produced is a result of an electron being ejected from an atom once a photon is absorbed and thus is referred to as the photoelectric effect^{1 2}. The phenomenon was explained by Einstein who treated the incident radiation as discrete packets of light called photons holding an energy of $h\nu$. If the value of $h\nu$ exceeds the work function of the material an electron has sufficient kinetic energy to be emitted. This is shown in equation 1 where E is the kinetic energy and ϕ is the work function of the emitter material³.

$$E = h\nu - \phi \quad (1)$$

3.1.2 Thermionic Emission & TECs

In 1901, Richardson continued the idea of the emission of electrons from materials and developed thermionic emission replacing the incident light with heat. He was awarded the 1928 Nobel Prize for his work with the thermionic phenomenon⁴. Similar to the photoelectric effect, electrons can leave the surface if they have thermal energy just equal to the work function of the material³.

Thermionic energy conversion (TEC) is one application of the thermionic effect. TEC uses the mechanism of thermionic emission for solar to electrical energy conversion. The idea was first proposed in 1915 by Schlichter, but developments in this sphere of research truly began to accelerate in the 1960s through to the 1980s. It was largely carried out by the space programmes of the US and USSR because of the high energy conversion rates and device simplicity that TEC technology offers. Unfortunately, TEC was eclipsed as a technology by cheaper alternative energy conversion methods such as photovoltaics. Following the availability of novel materials to improve operative methods the 21st century has seen a renewed interest in TEC. For the continuation of deep space missions and power generation technology it is necessary to keep exploring a wide range of alternative energy conversion

methods to replace fossil fuels ⁵. Novel renewable energy sources will advance growth and protect the world, without sacrificing one for the other.

TEC can be described as a heat engine; a simplified version is displayed in Figure 1a. The engine consists of a vacuum or a gas filled chamber with a hot cathode source as the emitter of electrons and a cold anode sink where the electrons are collected and give up their kinetic energy to do electrical work by virtue of their potential energy, in an external circuit ⁶. Figure 1b displays the corresponding energy level of an emitted electron.

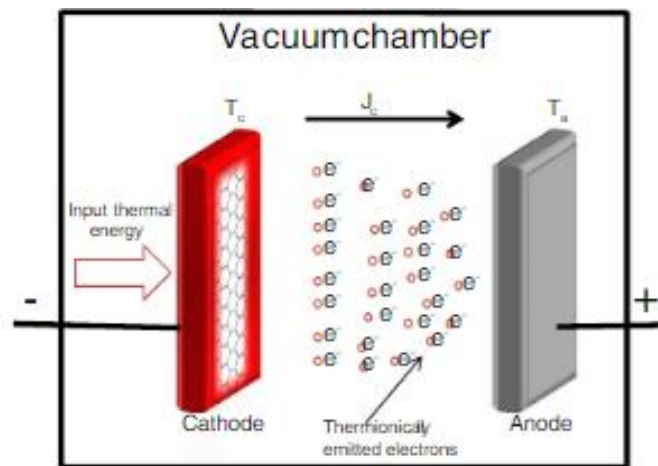


Figure 1a. Simplified schematic diagram of electrons emitted from the hot cathode (T_c) transferring to the cold anode (T_a) with the resulting current (J_c) ⁴.

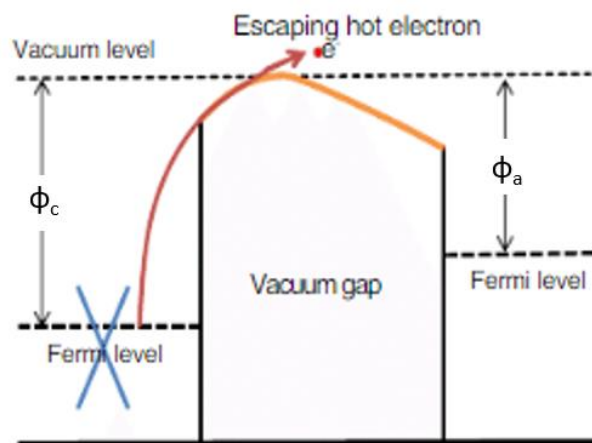


Figure 1b. An energy diagram following the path of an electron escaping into vacuum, where Φ_c & Φ_a are the work functions of the cathode and anode respectively. The orange line represents potential energy in the vacuum ⁴.

The efficiency of any 'ideal' heat engine is limited by the Carnot cycle, where to maximise efficiency, a large temperature difference between the anode and cathode is

required. This is shown by equation 2, where T_c is equal to the anode temperature and T_h is equal to the cathode temperature ⁷.

$$\text{Efficiency} = 1 - \frac{T_c}{T_h} \quad (2)$$

The emitter can be heated by either laser or a filament. Laser heating is advantageous in a laboratory setup as there is better temperature control and less current noise measured. Once heated, the electrons that have sufficient energy to overcome the work function barrier of the cathode can escape into the vacuum. A positive potential difference attracts the electrons through the vacuum towards the anode collector. The escaped electrons hold kinetic energy and approximately 30 times more potential energy. When in contact with the anode the electron loses energy proportional to the work function of the anodic material. Therefore, it is favourable to have an anode with a very low work function as the electron is free to use any remaining energy to do work in a connecting electrical circuit following this interaction.

Thermionic emission is described by the Richardson – Dushman equation. The saturated thermionic emission current density (J), is related to the temperature of the emitter (T) as shown in equation 3. Where e is elementary charge, h is Planck's constant, m is effective mass, k is the Boltzmann constant, and ϕ is the work function of the emitter ⁸.

$$J = \frac{4\pi m e k^2 T^2}{h^3} \exp\left(-\frac{\phi}{kT}\right) \quad (3)$$

Whereby under the same conditions of temperature and external electric field, decreasing the work function of the cathode material increases the emission current. The anode also has a low work function and would likewise emit electrons at a high temperature, this requires a large temperature difference to be maintained between the anode and cathode. The next sections of the introduction will discuss the applications and various limitations of the heat engine and how they can be modified to improve the efficiency of thermionic emission. Previous work will be examined, and the aim of this project will be outlined.

3.1.3 TEC Applications

TEC involves direct energy conversion with no moving parts, this allows for long lifetime devices with little maintenance required. Devices also produce high power outputs for small volume inputs and therefore acquire high specific power.

One extremely practical application of TEC is, when in combination with other systems, it is also able to convert unused waste heat energy. Photon enhanced thermionic emission was developed to increase the efficiency of standard solar cells. It combines both the photoelectric and thermionic effects by utilising the heat loss from the ejection of electrons when irradiated with photons to further excite more electrons across the band gap. PETE has received high attention recently for use in solar cells due to the promise that efficiencies of 60% and more can be achieved⁹. It has a great number of further applications such as cancer therapy, photo detection and solar energy converters¹⁰.

3.1.4 TEC Efficiency

When designing a TEC heat engine there are many other factors that need to be considered when trying to increase thermionic emission. Firstly, the inter-electrode gap between the cathode and anode can be a limiting factor. When in vacuum, there are two advantages; particle collisions are minimised, and the thermal insulation allows a heat difference between electrodes to be maintained. However, at certain current densities there can be a build-up of electrons in the gap which lack enough thermal energy to reach the anode. This creates a cloud of electrons blocking the gap, termed a ‘space charge barrier’, limiting the output current according to the Child-Langmuir law so that electron emission output no longer obeys the Richardson-Dushman relation⁵. There are four ways in which the space charge barrier can be mitigated;

- 1) Placing the anode and cathode as close together as possible (less than 10 microns)¹¹.
- 2) Counteracting the negatively electrons with positive ions⁶. For instance, ionised caesium gas serves two purposes upon introduction into the chamber. Firstly, the positive ions will be attracted to the negative space charge and it will be neutralised. Secondly, caesium has been shown to lower the work functions of both the anode and cathode⁶. It has also been demonstrated that methane provokes enhancement of thermionic emission as the molecule assists charge transfer across the inter-electrode gap¹².

- 3) The use of magnetic and electric fields to help the motion of electrons to the collector ¹³.
- 4) An inter-electrode grid to accelerate the electrons in a focused path to the collector ¹⁴.

Recent work from Bristol has looked at using two aligned grid electrodes in the gap between the emitter and collector. The first is closer to the emitter, the deflector electrode, and attains a small negative voltage bias. The other is positioned near the collector, the attractor electrode, and has a slightly larger positive bias. The use of the two grids in conjunction helps the motion of electrons to the collector. By modulating the voltage on the second grid the electrons are deflected minimising their loss to the attractor grid ¹⁴.

Another consideration is finding an emitter material that can withstand repeated cycling to high temperatures but retains a low work function for optimal emission. This has been a major obstacle that has caused the slow development of vacuum TEC technology during the 20th century. Recently, semiconductors have been introduced for use in TEC. Semiconductors, such as diamond, offer the huge advantage of adjustable work functions and electron affinities by incorporating other elements into the bulk and onto the surface.

3.2 Diamond

3.2.1 Properties

Diamond was first mined in Golconda, India approximately 4000 years ago. This region remained the sole producer of diamond up until the 18th century where diamond chips were discovered being used by local gamblers in Brazil and subsequent intense mining began ¹⁵. The original use for diamond was as a highly sought gemstone due to its hardness, rarity and sparkle that it possessed, with the word diamond originating from the Greek ‘adamas’ which translates as invincible ¹⁶. The properties that first made diamond so desirable, are also the reason for their popularity in many modern scientific and technological applications ¹⁷. A potentially novel application is the use of synthetic diamond as a high temperature low work function emitter material to enhance TEC performance.

Due to the valency of carbon there are many other metastable allotropes it can form alongside diamond as shown in Figure 2. Each structure has unique properties due to the different bonding and interactions involved.

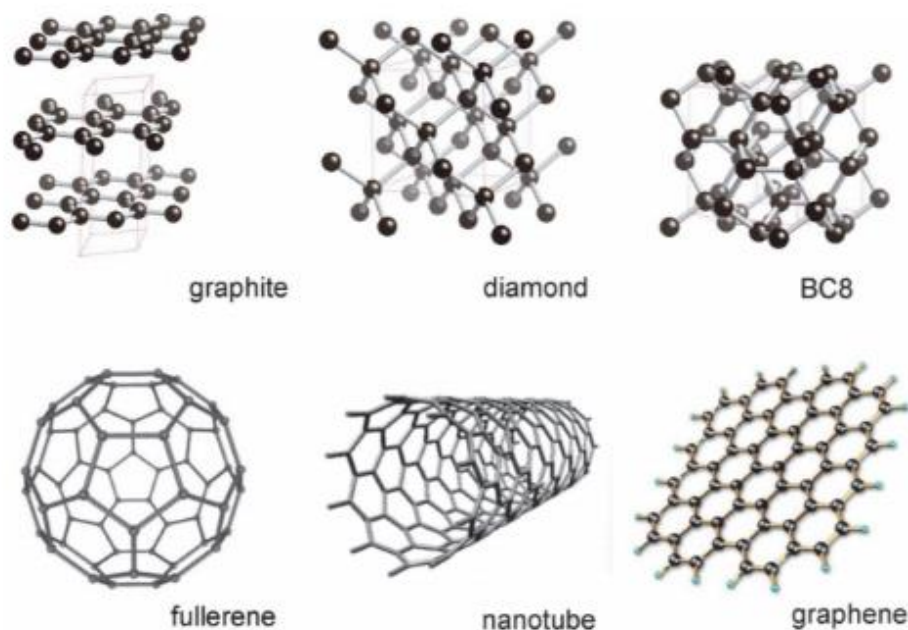


Figure 2. Structures of selected allotropes of carbon ¹⁸.

Two widely known allotropes of carbon are diamond and graphite which display a large difference in physical properties as shown in table 1. Diamond has a tetrahedral structure with each carbon bonded to four others producing sp^3 hybridised orbitals. The electronic configuration of carbon is $1s^2 2s^2 2p^2$, therefore once bonded there are no free electrons left in the structure making diamond a strong electrical insulator. In graphite each carbon is bonded to three others giving a hexagonal planar sp^2 hybridised structure. Although the carbon-carbon bonds are strong, there are weak Van der Waal forces between the hexagonal sheets causing graphite to be a lot weaker in structure. Graphite is electrically conductive due to the presence of delocalised π electrons present between the hexagonal layers. Under standard conditions, in the interconversion between diamond and graphite, diamond is the kinetic product and graphite is the thermodynamic product. Once diamond is formed the energy barrier to convert back to the more stable graphite is unfavourably high making the diamond metastable as shown in Figure 3. Without a catalyst, graphitisation of diamond only occurs with noticeable rates at temperatures greater than 2000 K ¹⁹. The energy barrier, E_1 , per atom is 3.5 eV ²⁰.

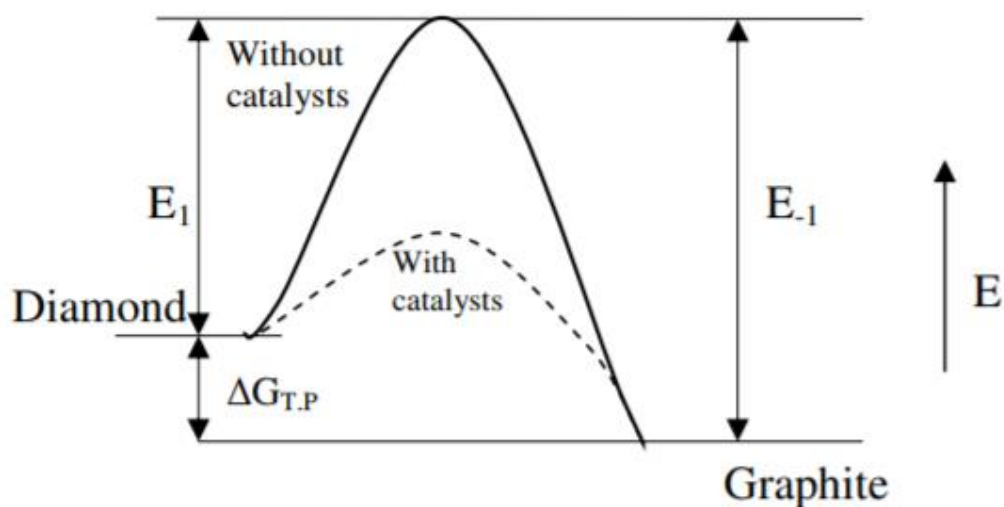


Figure 3. Energy diagram showing the activation barrier (E_1) in the conversion from diamond to graphite without catalysis, as well as the corresponding reverse conversion (E_{-1}). The dotted line represents the barrier with catalysts present ²¹.

Diamond is therefore used in many applications due to the strong compact structure that is thermally stable. Furthermore, it is dissimilar to other electrical insulators as it is highly thermally conductive and is particularly desirable due to the chemical inertness ideal for resistive coatings. Table 1 compares and contrasts the properties of diamond to graphite, highlighting the largely superior properties displayed by diamond.

Table 1. Adapted table of properties of diamond and graphite ^{22 23 24}.

Property	Diamond	Graphite
Crystal system	Cubic	Hexagonal
Orbital hybridisation	Sp^3	Sp^2
Covalent radius (pm^3)	77	73
Mohs hardness	10	-1
Heat capacity ($J mol^{-1} K^{-1}$)	6.155	8.517
Thermal conductivity ($W m^{-1} K^{-1}$)	2200	150
Resistivity (Ωm)	10^{12}	10^{-3} (c axis) 10^{-6} (a axis)
Atom density (cm^{-3})	1.14×10^{23}	1.77×10^{23}
Physical density ($kg m^{-3}$)	3510	2250
Electron Mobility ($cm^2 V^{-1} s^{-1}$)	2200	20×10^3
Band gap (eV)	5.45	-0.04

3.2.2 Synthesis

Diamond is naturally formed in the Earth's mantle at extremely high temperatures and pressures and brought to the surface via volcanic activity. Historically, diamond could only be acquired through prospecting geological deposits present on the Earth's surface and mining extinct volcanos. The cost and rarity of natural diamond has led to other fabrication methods to produce synthetic diamond for modern day industrial use.

The first method that was developed was the high-pressure high temperature (HPHT) method in 1955 by General Electric. It converts graphite to diamond and is designed to mimic the natural process of diamond formation due to the extreme conditions involved and the single crystal diamond produced. HPHT takes place in a hydraulic press with typical pressures of 5-10 GPa, temperatures of 1300-2300 °C and a metal catalyst. The graphitic carbon is left to be pressed and ensuing diamond crystallisation occurs ²⁵.

The chemical vapour deposition (CVD) method was subsequently developed in the late 1950s. It is advantageous due to the low operational pressures and temperatures saving energy and equipment cost. Furthermore, later developments allowed for the growth of diamond films, not just single crystals, whereby the grain size and doping of other elements into the carbon structure can be manipulated. This provides the ability to increase the conductivity of diamond which is beneficial for thermionic emission. Figure 4 compares the operative conditions for varying diamond production methods.

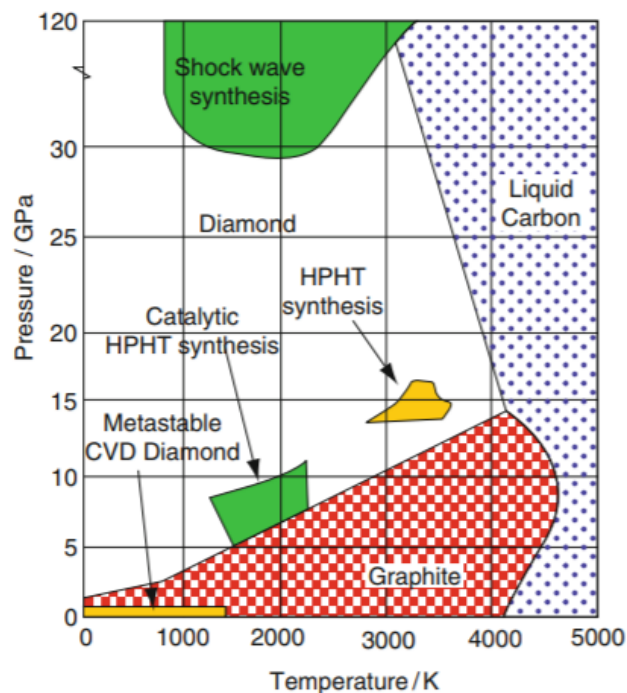


Figure 4. Phase diagram of carbon, showing the most stable form at each pressure and temperature ²⁶.

The idea of CVD is to add carbon atoms one by one in a tetrahedral pattern to a template forming diamond. There is a gas phase reaction of carbon containing molecules above the template providing the carbon to be deposited. However, up until the late 1960s progress was slow. Graphitic carbon is more thermodynamically stable than diamond and was consequently also being deposited on the surface. To prevent graphitic deposition Angus' group discovered the importance of incorporating atomic hydrogen with the precursor gaseous species. Atomic hydrogen causes the more stable diamond phase to dominate by stabilising the diamond lattice whilst etching away diamond like carbon and graphite. Furthermore, hydrogen breaks up the long hydrogen carbon chains in the gaseous mixture preventing them from adsorbing to the surface instead of diamond carbon. Often oxygen is incorporated into the mixture to greater improve the quality of the diamond film. The OH radicals that are subsequently produced etch away graphitic carbon at an even greater rate than the H²⁷.

During CVD, the carbon containing precursor molecules must be activated to produce carbon radicals. There are three methods to achieve activation that are dominant in the field; hot filaments (HFCVD), DC Plasma CVD, and microwave plasma (MPCVD). The first method involves a hot filament, such as tungsten, placed above a substrate and heated to around 2200 °C. The gas mixture flows across the filament where it is activated. The issues with HFCVD are mainly caused by the filament as it may sag over time or contaminate the diamond film²⁸.

The remaining two methods are both used in this report; MPCVD for growth and termination and DC CVD solely used as an alternative termination method. In both cases an electron field is used to rip electrons from the nuclei of hydrogen gas forming an electron plasma around the substrate. In DC CVD gases flow between an anode and cathode producing a high temperature discharge jet which is sustained by a direct current (DC) between the electrodes. DC Plasma CVD allows for quick growth rate relative to the other methods and is useful for mechanistic study²⁹. MPCVD creates a plasma using a microwave reactor at high frequency and power in a vacuum chamber. The electrons in the plasma resonate with the microwaves and the substrate is heated due to this microwave coupling as well as direct bombardment from the plasma. The advantages of MPCVD include the high plasma density, mitigation of electrode pollution due to the electrodeless process, and good quality films can be deposited for hours or days^{30 31 32}.

The substrate for diamond growth can be diamond also, this is defined as homoepitaxy; when substrate and material grown are the same. Heteroepitaxy is when a non-diamond substrate is used, such as silicon, molybdenum, iridium. In this case, in order for diamond to grow the substrate must be seeded by small diamond nanocrystallites^{31 33}. The ability to deposit diamond film on a variety of substrates has made it extremely useful and cost effective as a coating. For instance, diamond is a coating for implants and prostheses. It is bioinert so does not trigger a reaction from the immune system, and cells readily adhere to it³⁴. Diamond is often chosen as a cover for microelectromechanical devices, especially ones which require a torque, due to its excellent mechanical properties³⁵.

Figure 5 shows the mechanism of CVD using methane as the precursor carbon containing molecule and atomic hydrogen for diamond stabilisation. Methane is often used as it can be obtained with high purity and holds the same tetrahedral structure as the desired diamond. Initially, the unbonded 'dangling' bonds on the surface are rapidly terminated with hydrogen. The surface H atoms may be abstracted by the gaseous atomic H leaving a reactive site. Occasionally, a CH₃ radical may adsorb on the free site instead of another H atom. Diamond is formed when a different methyl group is also adsorbed at an adjacent site and forms a radical after further H abstraction. This radical can then attack the initial methyl group and the formation process is complete.

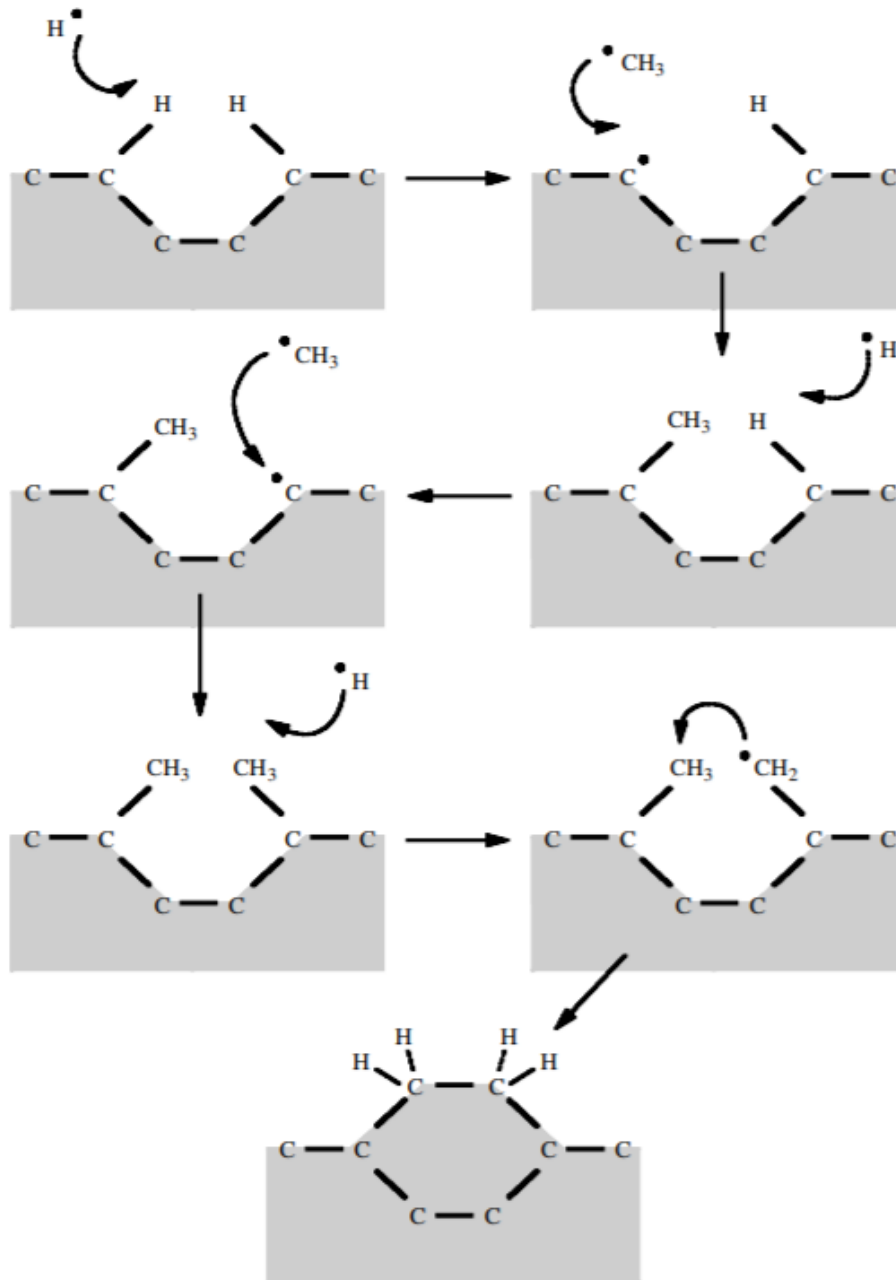


Figure 5. A simplified schematic diagram showing the adsorption of methyl radicals to the diamond surface and stepwise subsequent diamond growth ³⁶.

Upon changing the ratios and compositions of the gaseous species for CVD it is possible to produce different types and grades of diamond film with varying physical properties as shown in table 2. Microcrystalline diamond doped with nitrogen is synthesised in this report. The following sections will discuss the advantages of this type of diamond for thermionic emission.

Table 2. The different types of diamond and their corresponding properties that are available by changing the composition and ratios of the precursor gas mixture ³⁷.

Property	Single – Crystal Diamond	Nanocrystalline Diamond (NCD)			Ultranano crystalline Diamond (UNCD)
		NCD (grown with high methane – low quality)	NCD (grown with nitrogen for doping)	NCD (highest quality – grown with greater hydrogen)	
Growth Chemistry	H ₂ /CH ₄	H ₂ /CH ₄	H ₂ /CH ₄ /N ₂	H ₂ /CH ₄	AR/CH ₄
Hardness (GPa)	100	80	-	-	98
Surface roughness (nm)	Depends on preparation	50-100	20-30	5-30 (depends on film thickness)	5-25 (depends on nucleation density & film thickness)
Grain size (nm)	1-10000	50-100	5-15	5-100 (depends on film thickness)	2-5
Bonding Character	Sp ³	Up to 50% sp ²	10-15% sp ²	<0.1% sp ²	2-5% sp ²

3.2.3 Diamond film - grain size

There are two major factors that can influence the conductivity of diamond films; grain size and doping. These parameters are both altered by the ratio and composition of the gaseous species used during CVD as shown by table 2. The changes in mechanical properties that occur upon decreasing the grain size to the nanoscale are a consequence of carbon's unique ability to rehybridise ³⁸. Smaller grain sizes give rise to a greater number of grain boundaries present in the diamond film, and therefore the percentage of atoms situated at grain boundaries is higher. For instance, on the nanometre around 10% of atoms are in connection to the grain boundary ³⁹. The pure diamond sp³ carbon rehybridizes at grain boundaries to produce amorphous sp² graphitic carbon which in turn results in π bonded grain boundaries. The higher the quality of diamond the less grain boundaries that are present in its structure.

It is the grain boundaries that are responsible for the increase in electrical conductivity, emission and mechanical strength of nanocrystalline diamond films. The diamond film can be viewed as having pockets of pure bulk sp³ insulating carbon surrounded

by networks of electrical conductivity along the grain boundaries, and thus exhibiting a weakly ‘conductive’ property.

Figure 6 compares the local electronic density of states (DOS) for pure bulk diamond (dashed line) with that of grain boundary atoms (solid line). There is distinct band gap of 5.45 eV between the σ bonding and σ^* antibonding in pure diamond. Upon introduction of sp^2 hybridised bonds, and sp^3 dangling bonds at the grain boundaries, electronic states within the band gap appear. There is a lack of spatial connectivity between the sp^2 graphitic carbon producing distinct and localised states and not a continuous band in the DOS as seen with graphene. Therefore, although conductivity in NCD cannot be expected to be metallic-like, as seen with graphene, there is the possibility of a transition of electrons amongst these states making the effective band gap smaller than that of bulk diamond. Under favourable surface conditions this may increase the number of electrons emitted from the cathode and is extremely beneficial for the thermionic heat engine as it allows for a ‘colder’ cathode ³⁵.

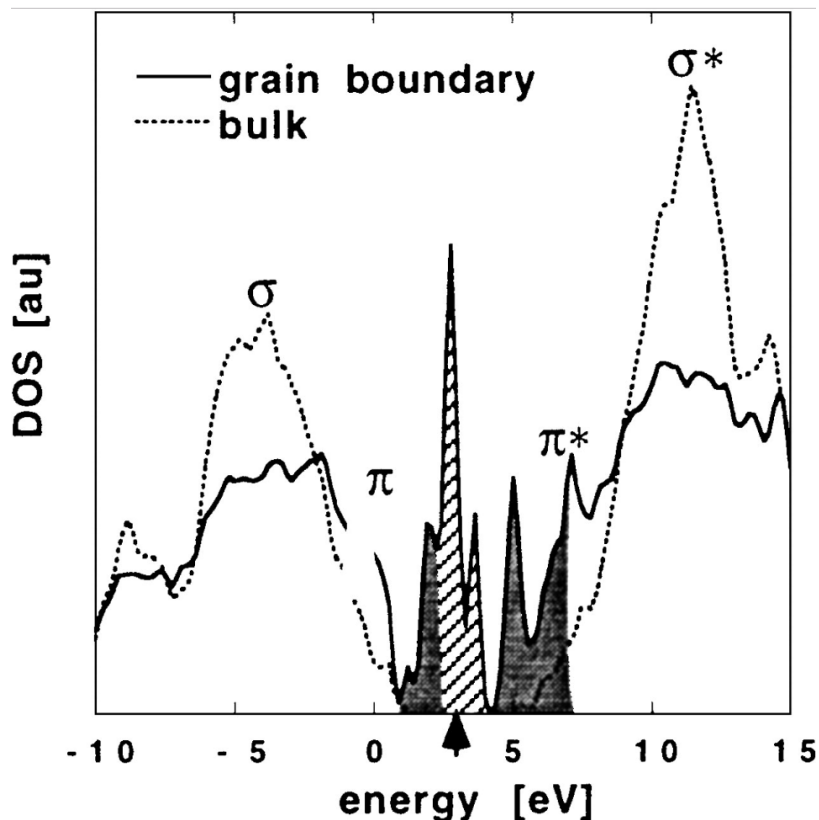


Figure 6. Bulk diamond band gap (dotted line) compared with the localised density of states (solid line) in the graphitic grain boundary region ³⁵.

3.2.4 Further applications

Another advantage of the ability to decrease grain size in diamond films is electron field emission which favours grain boundaries. Field emission studies undertaken at Bristol have looked at using an applied electric field to extract electrons from a diamond surface. Possible uses for this include the study of surface science and use in fast switching vacuum electronics ⁴⁰. It was demonstrated that samples with smaller grains and greater number of grain boundaries produce a higher emission current over the same uniform area than those with larger grains ⁴¹.

There is also the advantage of greater surface smoothness due to the small crystallite size. This makes diamond films useful for tribological applications. An example of a demonstrated tribological process using diamond films is surface acoustic waves (SAW). The smoothness of the film allows for the propagation of SAW without having to mechanically polish the surface ⁴².

3.2.5 Diamond films – doping

Electrically conductivity and thus the work function of diamond can be manipulated by the incorporation of other elements into the material and can be altered from highly insulating to near metallic ⁴³. Figure 7 shows a diagram representing the band structure of a typical undoped semiconductor. Diamond is an electrical insulator with a wide band gap of 5.45 eV between the valence band (VB) and the conduction band (CB), and therefore at low temperatures electrons are not able to jump to the higher CB levels.

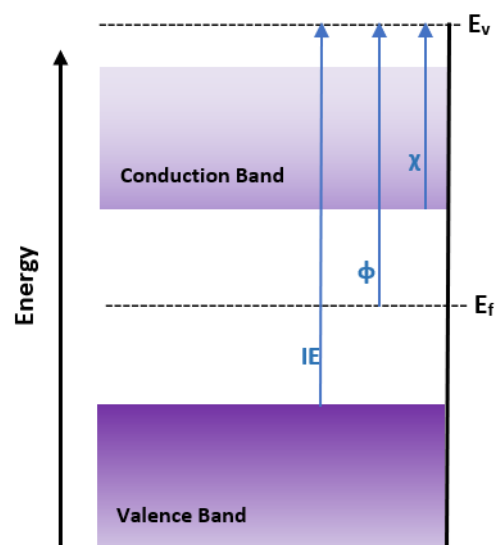


Figure 7. Band structure of a typical semiconductor, where IE is the ionisation energy, ϕ is the work function, χ is the electron affinity, E_v is the vacuum level and E_f is the fermi level.

The most common dopant elements in diamond along with their thermal activation energies are displayed in table 3. For *n*-type doping phosphorous has a lower activation energy than nitrogen and thus electrons would be able to jump from the VB to the CB at lower temperatures. However, diamond has a covalent radius of 77 and therefore the most similar in size is nitrogen. Nitrogen is therefore used for doping into diamond in this report despite its deep donor level as it substitutes more smoothly into the structure than phosphorous.

Table 3. Common doping elements and their properties ^{43 44}.

	Element	Activation Energy (eV)	Covalent Radius (pm³)
<i>n</i>-type	Nitrogen	1.7	71
	Phosphorous	0.6	107
<i>p</i>-type	Boron	0.37	84

Donor dopants are the *n*-type elemental impurities. Nitrogen and phosphorous have five valence electrons and therefore upon substitutional incorporation into diamond they form four covalent bonds with carbon, leaving one electron left over. Conversely, boron is trivalent and thus forms three bonds with carbon leaving an electron hole and is known as a *p*-type acceptor dopant. Therefore, the major charge carriers in *n*-doped diamond are electrons and in *p*-doped diamond are electron holes. Addition of these elements alters the Fermi level of diamond and consequently the conductivity as shown by Figure 8. Conductivity is increased from *n*-type dopants due to the smaller distance between the Fermi level and conduction band encouraging the donation of the weakly attached extra electron to the conduction band. The reduction in distance between the valence band and Fermi level to 0.37 eV from boron *p*-type dopant addition promotes the jump of electrons into the vacant hole at the Fermi level.

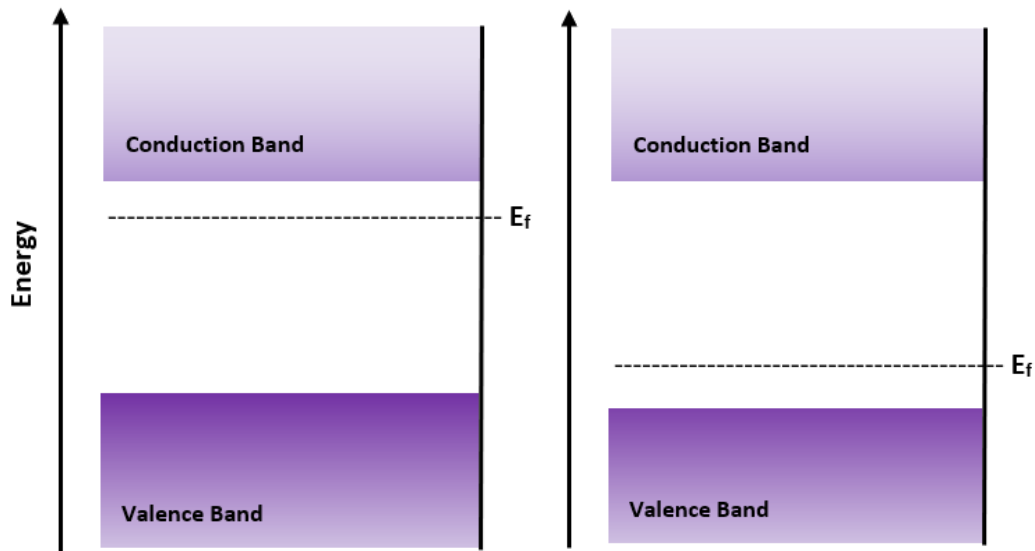


Figure 8. The alteration of the fermi level in a typical semiconductor upon addition of *n*-type dopants and *p*-type dopants respectively.

Band bending occurs upon doping due to the different morphology of atomic bonds on the surface of diamond as lattice periodicity is terminated. For instance, the ‘dangling bonds’ present on the surface are able to interact with one another forming graphitic sp^2 carbon bonds. As previously discussed, this produces local density of states within the band gap of diamond which differs in comparison to the bulk. When undoped, the fermi level of the diamond bulk is equal to that of the surface and remains flat as there is no charge transfer. When a semiconductor is *n*-type doped the Fermi level of the bulk is higher than that of the surface and electrons flow towards the surface until an equilibrium is reached. Upward band bending is observed to accommodate the alignment of the bulk and surface Fermi levels. This is the effect observed in this report due to the bulk being more ‘*n*-type’ than the surface. The opposite is seen with *p*-type doped semiconductors and electrons flow away from the surface inducing downward band bending. Figure 9 displays all three possible situations. The extent and direction of band bending is determined by the location, concentration, composition and charge of the dopants incorporated into the semiconductor.

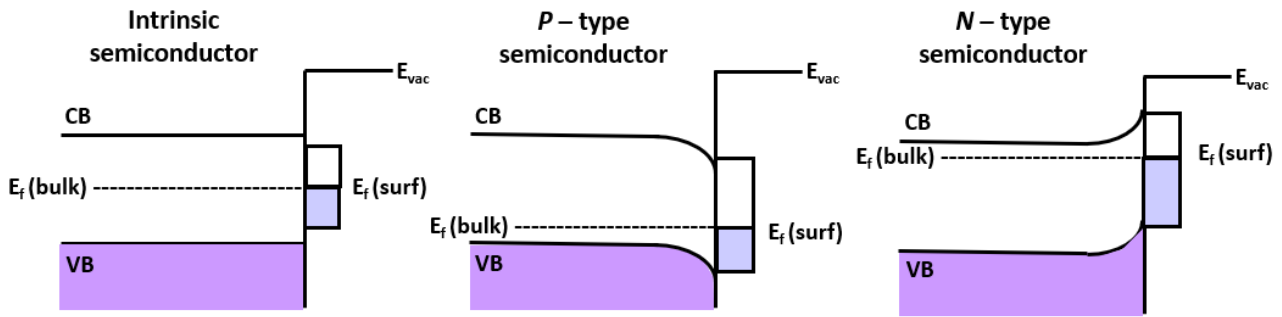


Figure 9. Subsequent band bending effects from the bulk of the material to the surface upon addition of dopants compared to that of an undoped material.

3.2.6 H termination

The previously discussed ‘dangling bonds’ on a clean surface of NCD are subject to reconstruction or termination in order to stabilise the unbonded electrons. Reconstruction involves the formation of an atomic bond between two sp^3 carbon dangling bonds producing sp^2 graphitic carbon. The second termination possibility is the adsorption of gaseous species on the surface. For instance, hydrogen termination on the NCD surface is another detrimental modification to improving efficiency of thermionic emission. It produces polarised C – H bonds increasing conductivity and resulting in a negative electron affinity (NEA). NEA is defined as when the vacuum level lies below the conduction band as shown in Figure 10. This lowers the ionization energy from 5.8 eV to as low 4.2 eV as a potential barrier for electrons to escape into the vacuum and again is a unique and beneficial property of diamond films allowing for a colder cathode ⁴⁵.

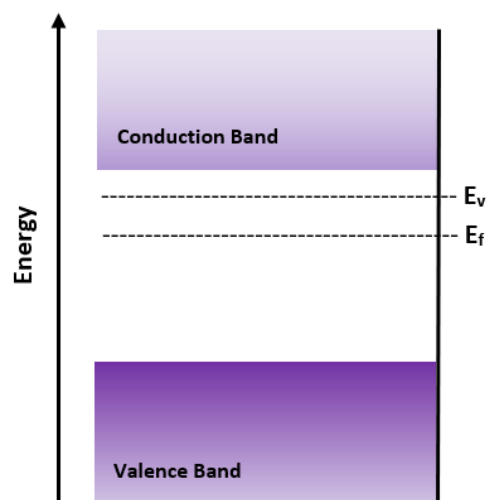


Figure 10. Simplified band diagram of hydrogen terminated diamond where the vacuum level now lies below the conduction band producing a negative electron affinity.

There is another band bending effect that comes into play upon adsorption of hydrogen atoms onto the surface of diamond. Due to the free carrier density of semiconductors being significantly lower than that of metals; 10^{17} cm^{-3} compared to 10^{22} cm^{-3} , the effective screening of the electric field produced at the surface is a lot lower in diamond. Hydrogen has a lower electronegativity of 2.2 compared with that of carbon at 2.55 resulting in a dipole at the diamond surface. The corresponding electric field of the surface dipole can penetrate approximately 100 \AA into the diamond which in turn produces a subsurface space charge region. Figure 11 shows diagrams for the space charge regions for a *n*-type semiconductor with electrons as the majority charge carriers⁴⁶. Depending on the orientation of the dipole is what depicts the nature of the space charge region and band bending.

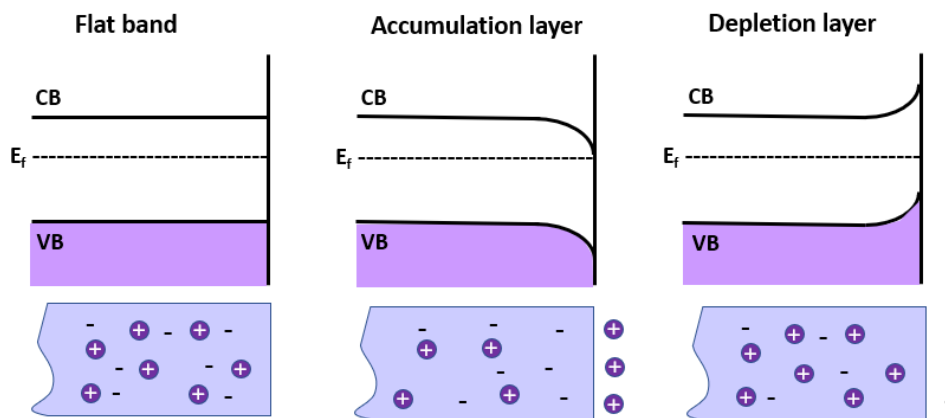


Figure 11. Band bending effects from the adsorption of species on the surface and the corresponding build-up of charge. For clarity, band bending effects from doping are not considered here⁴⁶.

In the case of hydrogen termination on a diamond surface an accumulation layer is formed due to the build-up of electrons just below the surface. H-terminated diamond displays a *p*-type surface conductivity due to the downward band bending, this is shown in Figure 12⁴⁷. There is the possibility of adsorbing other molecules onto the surface such as hydrocarbons where electrons can be donated from the diamond into the LUMO of the adsorbed molecule leaving a subsurface electron hole accumulation, this is known as surface transfer doping^{47 48}. This allows for a controlled and non-destructive method of doping which is useful for organic and nanoelectronics⁴⁹.

Diamond (111) 1x1:H

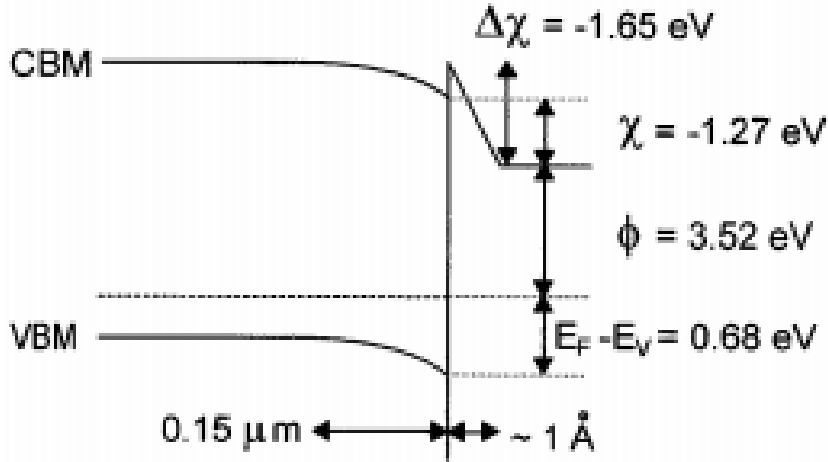


Figure 12. Band diagram of hydrogen saturated diamond with a negative electron affinity, where $0.15 \mu\text{m}$ is the depletion layer and 1 \AA is the surface dipole layer. Doping band bending effects are omitted for clarity ⁵⁰.

The band bending effects from both doping and surface terminations can be combined to interact constructively and destructively with one another. In the case of hydrogen terminated nitrogen doped diamond, as discussed in this report, the effects combine destructively and are presented on Figure 13. Upon addition of hydrogen the degree of upward band bending is reduced, and an NEA is formed.

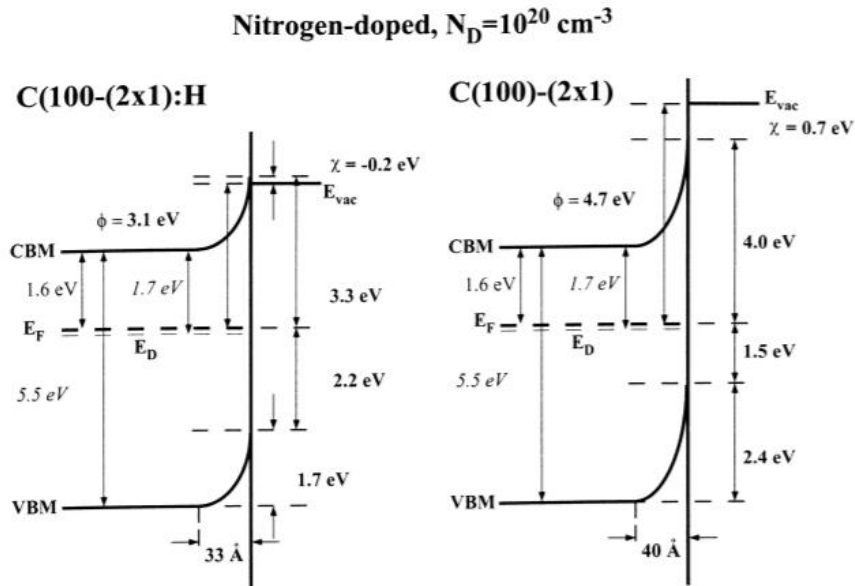


Figure 13. Work undertaken by Diederich et al where the left Figure shows the combined effects of nitrogen doping and hydrogen termination on band bending. Note the upward band bending is less heightened and the introduction of the negative electron affinity in comparison to the right Figure ⁵¹.

Unfortunately, as we heat the diamond to temperatures above 600°C the hydrogen begins to desorb, limiting the electrical current output. Studies are underway to resolve this involving low pressure hydrogen operating environments in order to increase the thermal stability at higher temperatures⁵². Another possible solution looks at using metal oxide terminations that are said to provide a stable NEA diamond surface⁵³.

3.2.7 Schottky Junction

Energy harvesting is a method of building up and utilising low grade energy that would otherwise be wasted. It is extremely advantageous to exploit, particularly with the digitalisation of society and the high volumes of wireless devices that come with it. One such example is the internet of things (IOT), which is the increased connection of devices. IOT relies on large amounts of low-powered wireless devices. For widespread implementation of these wireless networks, energy harvesting is required⁵⁴.

A Schottky diode is a highly efficient method for harvesting energy. It is formed from the contact between a *n*-type or *p*-type semiconductor, such as diamond, and a metal. Often *p*-type diamond is preferred to make Schottky diodes due to the poor semi conductivity of nitrogen or phosphorous doped diamond at room temperature. The semiconductor acts as the cathode and the metal as the anode. Conventional current can only flow from the metal to the semiconductor when a forward voltage is applied. The advantage of Schottky diodes over typical semiconductor – semiconductor diodes is the lower forward voltage producing low power input devices with high efficiency⁵⁵.

3.2.8 Characterisation

The scanning electron microscope (SEM) is the non-destructive characterisation method used in this report. SEM involves a high energy focused electron beam directed at the surface of the sample. The beam interacts with species on the surface and induces a variety of physical processes collectively termed ‘scattering events’. The individual events such as backscattered electrons, secondary electrons and x rays all convey information about the sample. Features such as morphology, orientation, crystal structure and local electrical and magnetic fields can all be deduced. It is the secondary electron emission, induced by the backscattered electrons, that displays the readable SEM image. Diffracted backscattered electrons yield information about crystal structures and orientations and adds to the SEM image. The X-rays released when excited electrons return to lower energy states are characteristic to each atom species ^{56 57}.

SEM imaging is highly useful, it allows grain size to be measured, as well as the observation of any surface defects and the extent of diamond growth on the substrate. Diamond grown by the MPCVD gives a variety of orientations, displayed in Figure 14. Triangles observed on the SEM image correspond to $\{111\}$ -textured diamond and squares observed correspond to the more desired $\{100\}$ -textured diamond. $\{100\}$ -textured diamond growth is largely pursued due to the superior optical and mechanical properties such as low roughness and high wear resistance it holds over the other orientations ⁵⁸.

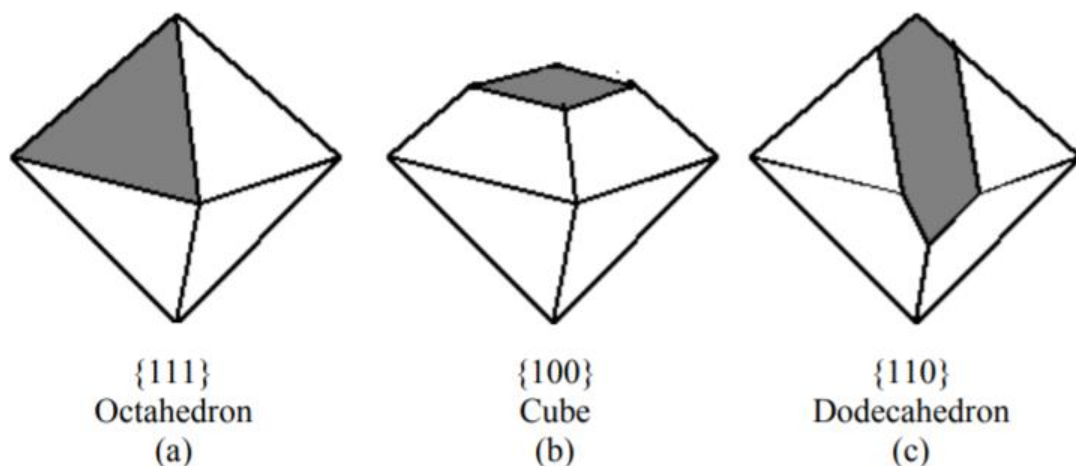


Figure 14. Schematic diagrams to show the $\{111\}$, $\{100\}$, and $\{110\}$ planes on an octahedron diamond ⁵⁹.

3.3 Beta enhancement

3.3.1 Radioisotopes

Since the dawn of nuclear energy as a renewable energy source there has been a boost of energy conversion or storage devices that rely on the decay of radioactive isotopes. For instance, Radioisotope Thermoelectric Generators (RTGs) convert the heat produced in decay into electricity. Other devices use the radiation such as gamma rays, alpha particles, or beta electrons emitted in decay processes in order to stimulate energy production. One radioactive source that has recently seen high usage in electricity generation is Nickel 63. ^{63}Ni is a radioactive isotope of Nickel that upon decay emits a beta electron of average energy 17.3 keV ⁶⁰.



^{63}Ni has boosted in popularity due to its long half-life of 100 years extending potential lifetime of power sources to this time, as well as it being below the radiation damage threshold of many semiconductors ⁶¹. Due to radioactive decay processes occurring regardless of external energy inputs radioisotope devices also have the ability to work in places that are inaccessible by harvestable energy. A prime example is using ^{63}Ni beta electrons to power sensors in remote locations such as the far North, deep sea or outer space. RTGs have also demonstrated reliability in powering space missions including the Apollo lunar missions ^{63 64}.

The technological application of nuclear batteries first came about in the 1950s ⁶⁵. However, there were public safety concerns and the first prototypes were soon shelved ⁶⁶. There has since been a revitalised outlook on radioisotope batteries, particularly in the 21st century. One such example is betavoltaic batteries which directly convert beta electrons into electricity. In 2016, the University of Bristol developed a betavoltaic diamond battery using ^{63}Ni as the radioactive source ⁶⁷. This has potential of replacing conventional batteries in situations where it is not feasible to replace easily. One suggested example would be implementation as a pacemaker. The low energy radiation, long lifetime, ability to work on the nanoscale and the bioinert diamond would make this device ideal.

3.3.2 Previous Studies

Previous work conducted by the Bristol Diamond Lab Group have looked at the effects of using ^{63}Ni to enhance thermionic emission. This was achieved by incorporating ^{63}Ni into the anode of the TEC set-up and using hydrogen-terminated nanocrystalline diamond (HTND) on a molybdenum substrate emitter. The following mechanisms for the increase in thermionic emission were discussed and assumed unlikely ^{68 69}:

1) Direct collection of beta electrons by the anode:

The emitted beta electrons are collected directly along with the thermionic emission electrons. This was discarded as the background current reading in the collector was the same with and without the ^{63}Ni .

2) Perturbation of the space charge region:

The high energy beta electrons interact with the low energy electrons in the space charge barrier region between the emitter and collector. The interaction lowers the energy required for the electrons to reach the collector.

3) Hydrogen desorption:

Beta or secondary electrons cause the desorption and subsequent ionisation of H atoms on the surface. This adds an ionic H- component to the current. However, it is more likely H+ ions will be produced which would in fact lower the current.

4) Alteration of bulk or surface:

Beta induced defects in the bulk material may increase conductivity or lower the work function at the surface increasing thermionic emission. However, any vacancies or defects are more likely to decrease the strength of the adsorbed H atoms on the surface. This would decrease the dipole strength, raise the work function and decrease the current produced.

The following mechanisms were discussed and deemed likely ^{68 69}:

5) Secondary electron emission (SEE):

The high energy beta electrons that reach the surface transfer enough energy to the surface electrons for subsequent emission.

6) Radiation induced conductivity (RIC):

The high energy beta electrons interact with valence electrons in the emitter material promoting the electrons to the conduction band and forming electron hole pairs. This increases the number of free carriers and therefore the conductivity in the material and boosts thermionic emission.

The semiconductor properties, low atomic number, high electron density, thermal stability, and chemical inertness of diamond contribute towards the high energy conversion efficiency during the interaction with beta electrons ⁷⁰. ⁶³Ni is an ideal candidate compared to other isotopes for the production of beta electrons; it has no accompanying gamma radiation, weaker bremsstrahlung (less radiation protection required), and the average beta energy will not damage the semiconductor ⁷¹.

3.3.3 The aims of this study

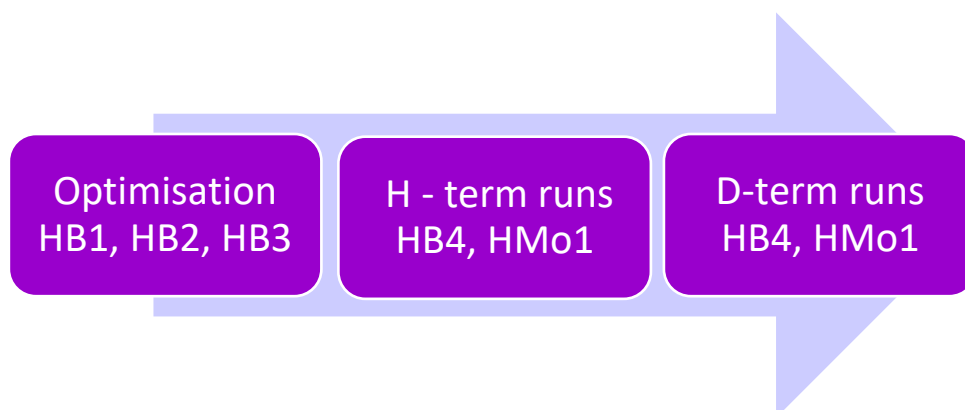
There is high potential for the harvesting of low-grade radioactive decay energy by the use of diamond Schottky diodes. These devices would combine the advantages of low power, little maintenance and long-life times for applications such as wireless power transfer. In order to develop this idea, the interaction of beta electrons with *n*-type diamond is further examined in this report.

To follow on from previous experiments, the aim of this report is to incorporate the ⁶³Ni into the cathode of the TEC with the expectation that the closer contact between the isotope and emitter will boost thermionic emission. Beta electrons are limited by how far they can travel through various media and have an energy dependent range, this must be considered when implementing ⁶³Ni into devices or in the future ¹⁴C into devices.

4 Experimental Procedures

4.1 Overview

Overall five samples were prepared; four diamond on diamond samples (HB) and one diamond on molybdenum sample (HMo). The first three diamond samples were used for optimising the preparation of samples. The remaining samples were used for experimental runs.



The initial considerations for the sample emitter were as follows;

- 1) The ^{63}Ni needs to be incorporated underneath the emitter.
- 2) The beta electrons need a way to reach the high-quality diamond at the surface of the emitter.
- 3) There needs to be a thermal vacuum between the sample and the ^{63}Ni during beta enhanced experiments as to not degrade the isotope.

The following sections will outline the conditions used for the preparation of samples. Section 6.1 discusses the reasoning behind the final conditions chosen.

4.2 Sample Preparation

4.2.1 Diamond

Figure 15 displays the three steps in preparing the diamond samples. A 10×10 mm element 6 thermal grade TM180 polycrystalline diamond template was chosen initially as it mitigates the need for a seeding step to stimulate diamond growth in the MPCVD. The first growth step provides a layer of low-quality diamond which serves two purposes. Firstly, it can effectively absorb the radiation heat during thermionic runs and thus the whole emitter is heated. Subsequently, less heat is transferred through to the collector and prevents it thermally expanding. In the second step, holes were milled through the diamond for the beta electrons to reach the high-quality surface diamond produced in the final growth step.

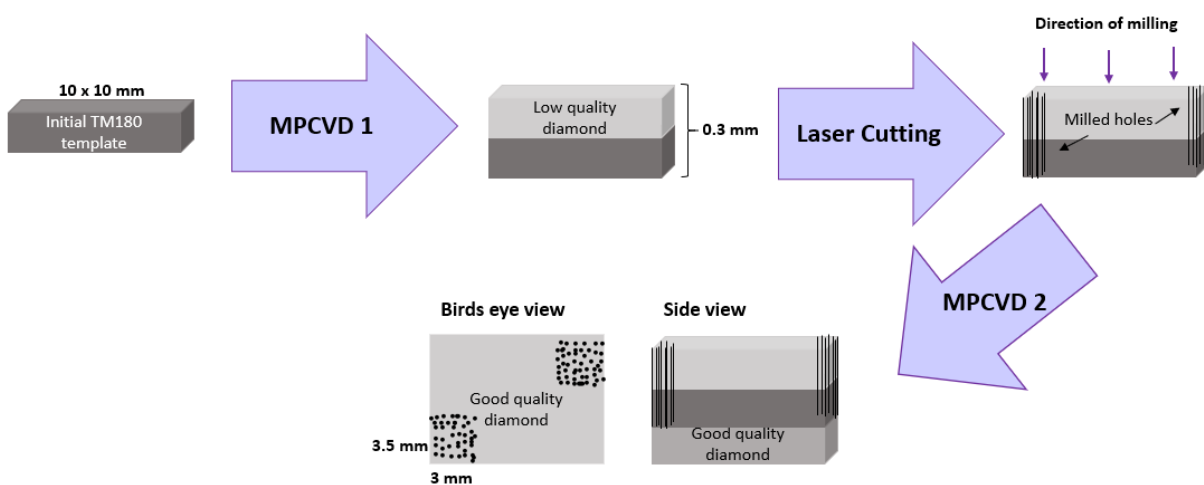


Figure 15. Diagram to show the three steps required in diamond sample preparation.

Step 1 - CVD 1

Firstly, low quality diamond is grown on the TM180 diamond template using the MPCVD. The decreased thermal conductivity of low-quality diamond allows for greater heat absorption from the laser. Heat is primarily transferred through phonons in diamond. In low quality diamond there is increased phonon scattering from grain boundaries, Umklapp processes, crystal defects and impurities. The increased scattering prevents the transfer of phonons and therefore heat across the diamond ⁷².

Figure 16 is a picture of the microwave reactor on the outside, during a H termination. Figure 17 shows a simplified version of the sample placement inside the reactor surrounded by the electron plasma during growth. The electron plasma is formed from a 1.5 kW ASTeX Magnetron which generated 2.45 GHz microwave radiation inside a 1 L cylindrical vacuum chamber. The conditions used for the growth of low-quality diamond are outlined in table 4. Tuning the microwave input is necessary to minimise the reflected watts from the radiation which when too high can cause damage to the sample and reactor. Extremely high temperatures are reached; therefore, the reactor has an inside water coolant system as well as cold air blowing through the walls. The temperature of the substrate is measured by the Raytek Thermalert SX optical pyrometer of which the emissivity is set to 0.13 when working with diamond samples.

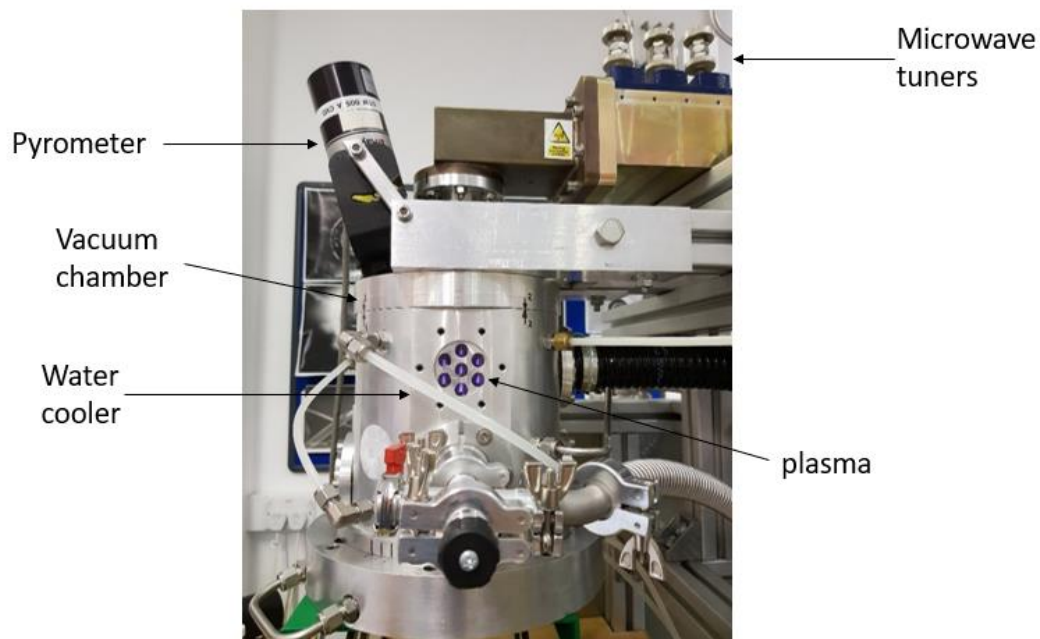


Figure 16. Labelled picture of the microwave reactor during a H termination.



Figure 17. The left picture shows a view of the plasma during a H termination. The right diagram shows a simplified set up of the sample inside the vacuum chamber surrounded by the electron plasma.

Table 4. MPCVD conditions used for growth of low-quality diamond.

Gas composition ratio			Power / W	Pressure / Torr	Temperature / °C	Time / hours
H ₂	CH ₄	N ₂				
89	10	1	1400	150	1130	2

Step 2 - Laser cutting

A 532 nm pulsed laser was used to mill holes in two opposing corners of the sample. Software is designed to move the laser in the x y and z directions. After optimisation the following program was developed to mill a 3 x 3.5 mm array of holes.

Table 5a. Program developed for the X and Y direction of the laser.

Direction	Number of holes	Spacing between holes / mm	Distance/ mm
X	100	0.03	3
Y	117	0.03	3.5

Table 5b. Program developed for the Z direction of the laser.

Direction	Number of steps down	Spacing between steps / mm	Dwell time on each step / s
Z	50	0.006	0.1

The diamond sample was milled under an oxygen atmosphere to provide a much cleaner cut as the oxygen burnt off any residual carbon as CO₂. When the sample was milled in air without an oxygen atmosphere, large amounts of sediment were observed around the holes. The sediment was comparable to the following SEM image of silicon cut in air during preliminary testing of the program, and had to be removed so as to not hinder the movement of beta electrons.

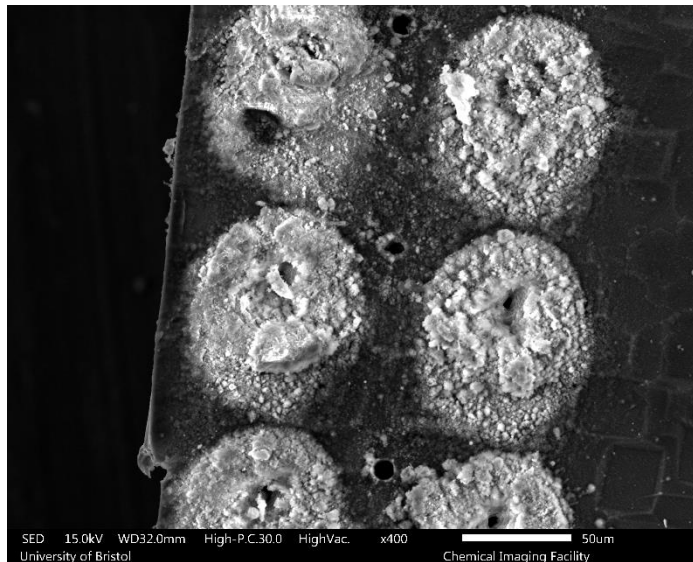


Figure 18. SEM image during preliminary laser cutting testing with silicon.

Step 3 - CVD 2

A further growth of nanocrystalline good quality electrically conductive diamond in the MPCVD is required for thermionic emission. Gas composition plays a large role in altering the quality of the diamond grown. In this case, the larger ratio of hydrogen gas in the reactor in comparison to methane and nitrogen causes the enhancement of conductivity. The greater density of grain boundaries, presence of graphitic carbon, and inclusion of nitrogen provide the local density of states and band bending facilitating the movement of electrons from the emitter to the collector ideal for thermionic emission. The diamond is deposited on the opposite side to where the holes were milled from. A growth time of one hour is required to cover the holes sufficiently with a layer of conductive diamond.

Table 6. MPCVD conditions for growth of high-quality diamond. Note the increase in H gas ratio.

Gas composition ratio			Power /	Pressure /	Temperature /	Time / hours
H ₂	CH ₄	N ₂	W	Torr	°C	
1000	41.7	1	1400	140	900	1

4.2.2 Molybdenum

Following experimental runs with the diamond sample, a 10 × 10 mm molybdenum sample was prepared. The purpose of this sample was to achieve greater thermionic emission owing to the more conductive molybdenum. Molybdenum is a suitable substrate owing to its high melting point, high thermal conductivity, strong carbide, and low coefficient of thermal expansion, which minimizes the mechanical stress on the diamond film⁶⁸. Figure 19 shows the three steps in preparing the molybdenum sample. Although an initial growth of low-quality diamond is not required, the molybdenum needs to be etched by the laser cutter in order to undergo radiative heating during TEC. Additionally, as the substrate is now heteroepitaxy an additional seeding step is required in order to stimulate diamond growth on the molybdenum.

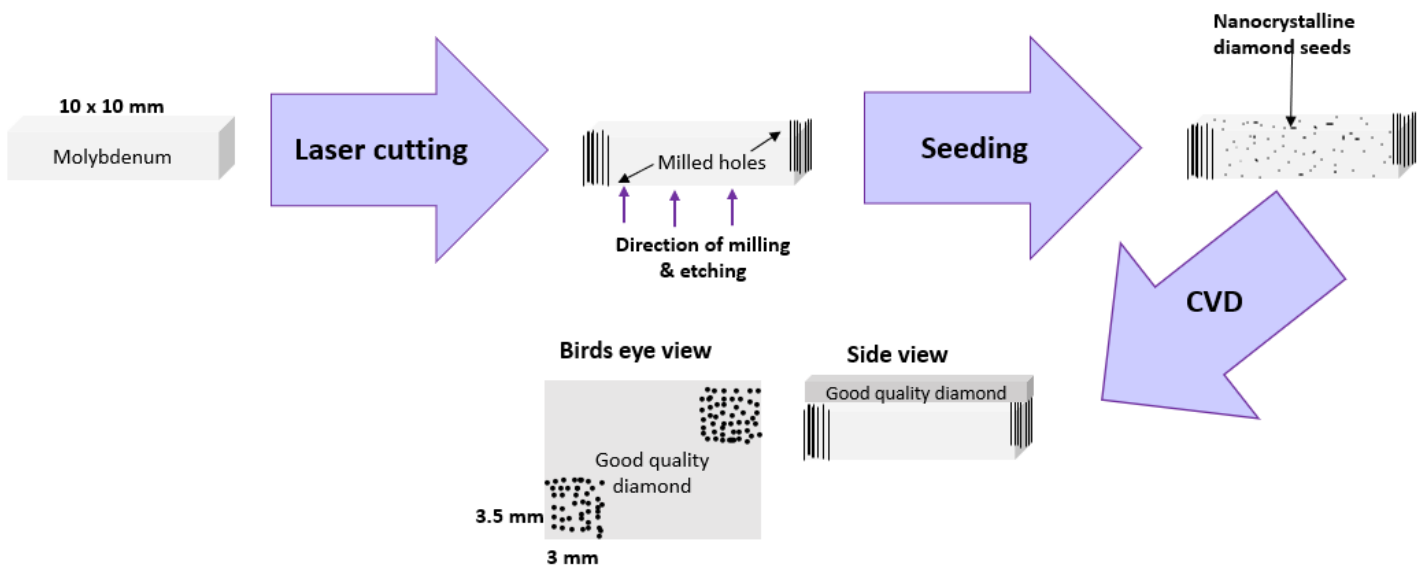


Figure 19. Diagram to show the 3-step process in preparing a molybdenum sample. Differing from diamond with the reduction of a growth stage but the addition of a seeding step.

Step 1 - Laser cutting

The molybdenum is approximately 0.1 mm thickness, allowing for fewer steps and a much shorter dwell time on each step compared to the diamond. The X and Y settings remained the same as for the diamond sample.

Table 7. Alteration of the program for the Z direction.

Direction	Number of steps down	Spacing between steps / mm	Dwell time on each step / s
Z	20	0.005	0.075

Molybdenum is a refractory metal and therefore it is difficult to radiatively heat, to solve this the sample needs to be etched using the laser cutter in order to absorb heat during TEC. Gratings were scribed on the same side as the holes are milled from using the laser cutter, this creates microstructures of similar size to the photon wavelength of the laser used in TEC. This enables the photons to resonate with the gratings and the sample can radiatively heat.

Step 2 – Seeding

In order to stimulate nucleation, the molybdenum must be seeded with nanocrystalline diamond pieces. This is achieved by submerging the substrates first in a carboxyethylsilanetriol di-sodium solution (25 %, Fluorochem) and then a suspension of sonicated 18 nm diamond (25 cts/kg, Microdiamond) ⁶⁹.

Step 3 – CVD

Conditions for the growth of good quality diamond mirrored that of the diamond sample. The only difference was an extra 30 minutes was required to cover the holes to the same degree. This could possibly be due to nucleation from nanocrystalline seeds takes longer than from a diamond template. The emissivity of the pyrometer was set to 0.25 as it is a molybdenum sample.

Table 8. MPCVD conditions for the growth of good quality diamond. Note the extra time required for the molybdenum sample.

Gas composition ratio			Power /	Pressure /	Temperature /	Time / hours
H ₂	CH ₄	N ₂	W	Torr	°C	
1000	41.7	1	1400	140	900	1.5

4.2.3 H-Termination

Before every run each sample was re-hydrogen terminated as the samples were being heated to temperatures high enough for hydrogen desorption to occur. Initially, the MPCVD was used for termination and provided consistent results. However, due to technical difficulties the DC CVD was also used to achieve hydrogen terminations. The conditions for each varied and are as follows;

Microwave reactor

There are three stages, all conducted under a hydrogen only atmosphere. The first stage is used to ‘clean’ the surface using high temperatures to desorb any molecules that may have been left on the surface. The second stage uses lower temperatures to adsorb a layer of hydrogen to the readily clean surface producing the NEA-inducing dipole. The final cooling stage is under a 30 Torr hydrogen atmosphere ensuring no other species can absorb in any remaining sites.

Table 9. MPCVD reactor conditions at each stage during a H-termination.

Stage	Temperature / °C	Power / Watt	Pressure / Torr	Time / minutes
1	890	1100	70	2
2	550	60	40	2
3	-	-	35	2

DC Terminator

The DC reactor was limited to a maximum temperature of 300°C due to the possibility of the plastic around the thermocouple melting at higher temperatures. Previous work with the DC terminator had varied the temperature, pressure, and voltage across the electrodes in order to find the optimal conditions for hydrogen termination. The water contact angle for each variation was measured and compared to the angle found on hydrogen terminated surfaces produced by the MPCVD. Due to the hydrophobic C-H bond the contact angle for a hydrogen terminated diamond surface is expected to be 90°⁷³. Initially, the hydrogen terminations were carried out at a low temperature and pressure of 150°C and 1 Torr for 10 minutes as these conditions had been found to yield the most similar angles to the MPCVD.

However, these conditions proved not to be as effective following subsequent thermionic tests. The temperature was then increased to 300°C at 1 Torr for 10 minutes which also proved to be ineffective. It can be determined that the role of temperature for hydrogen termination is detrimental, and whilst the DC reactor cannot surpass 300°C effective surface termination is not possible.

4.2.4 Deuterium Termination

In the interest of time, both samples were terminated with deuterium in the MPCVD and the effects on thermionic emission looked at rather than beta enhancement with the molybdenum sample. The deuterium termination was conducted under closed cycle conditions instead of a constant flow rate of gas through the chamber. This was done in order to save the deuterium for future use. All the other conditions mirrored that of the hydrogen termination. For direct comparison a hydrogen termination on both of the samples was also carried out under closed cycle conditions.

4.3 Measuring emission

4.3.1 Experiment Set-up

The complete set-up for TEC experiments is displayed in Figure 20. The emitter was held under vacuum and radiatively heated from below by a polarized Synrad Firestar 40 Watt CO₂ laser. A Land SPOT R160 optical pyrometer was directed at a mirror reflecting to the bottom of the sample in order to accurately read the temperature. There is a small gap of 300 μm between the emitter and collector controlled by a linear motor (Z825V, Thorlabs, Germany). A 31 V bias across the two electrodes ensured any emitted electrons would contribute to the measured current. Quartz is electrically and thermally insulating and so is used as the sample stage to hold the emitter.

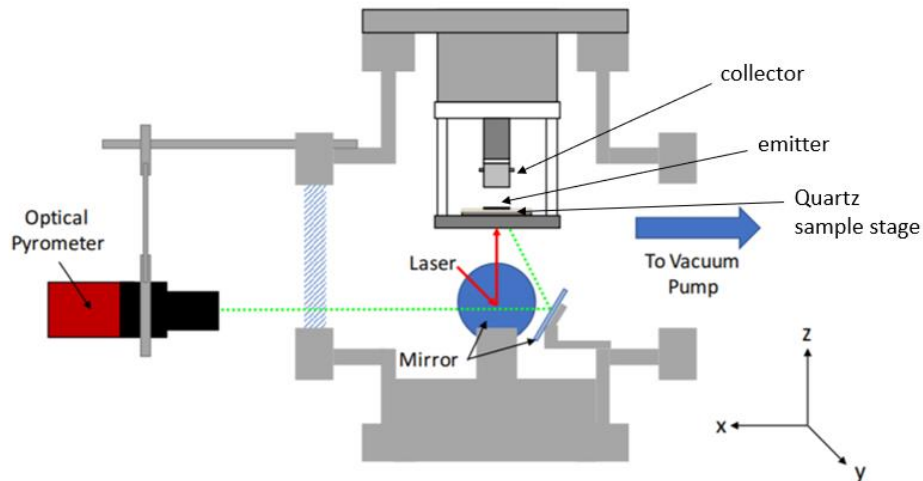


Figure 20. Adapted diagram showing the overall TEC set-up ⁶⁹.

4.3.2 Emitter Set-up

The arrangement of the emitter for experiments alternated with and without the inclusion of 3 x 3 mm ⁶³Ni (2.6 MBq) as shown by Figure 21. The quartz provided a vacuum between the ⁶³Ni and the sample, and therefore when the sample was heated up the ⁶³Ni remained thermally insulated. The milled holes in the opposing corners ensured the ability of the beta electrons to reach the surface.

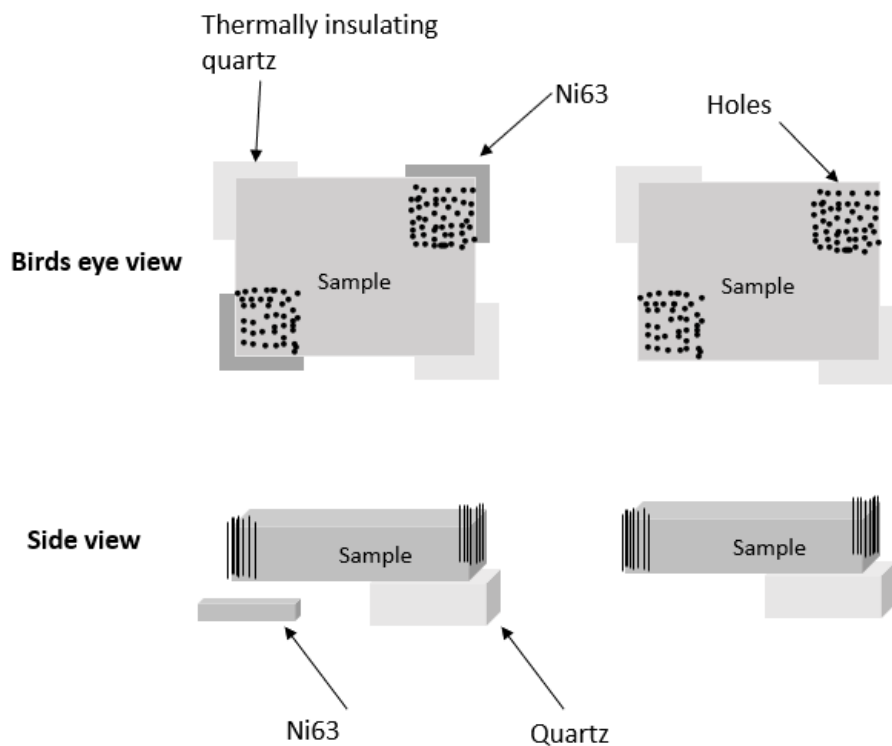


Figure 21. View of the sample with and without incorporation of ⁶³Ni underneath the milled holes.

5 Methodology

5.1 Experimental Runs

Overall, there were two samples prepared; a diamond on diamond HB4 sample, and a diamond on molybdenum HMo1 sample. Each sample underwent several TEC runs, with the inclusion of ^{63}Ni alternating between runs.

Run	1	2	3	4	5	6	...
Beta?	-	β	-	β	-	β	...

Table 10 shows the number of runs undertaken by each sample in the order in which they were taken. The type of termination used and the method for termination is also outlined. The unsuccessful thermionic experiments using the DC terminator suggest hydrogen termination was not achieved.

Table 10. Table to show the order of experiments with each sample and whether thermionic emission was observed.

Sample	Termination	Reactor	Number of Runs	Successful TEC?
HB4	H	MPCVD	13	Yes
HB4	H	DC CVD – 150°C	2	No
HMo1	H	DC CVD - 150°C	2	No
HB4	H	DC CVD - 300°C	1	No
HMo1	H	DC CVD - 300°C	1	No
HMo1	H	MPCVD	1	Yes
HMo1	D	MPCVD (closed cycle)	1	Yes
HB4	D	MPCVD (closed cycle)	1	Yes
HMo1	H	MPCVD (closed cycle)	1	No
HB4	H	MPCVD (closed cycle)	1	Yes

Figure 22 shows the temperature profile for each run. Current was measured as the sample was heated from 300°C to 600°C. The temperature remained at 600°C for 3 minutes

before decreasing back to 300°C. Temperatures greater than 600°C were not used as to not cause too much damage to the sample so that it could be used for multiple runs.

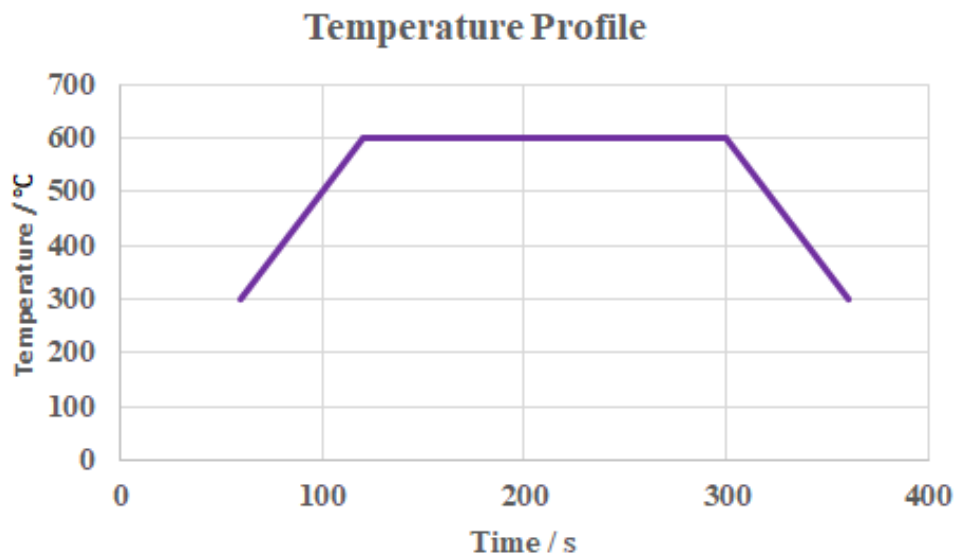


Figure 22. Graph to show the temperature profile of the sample during a run.

6 Results / Discussion

6.1 Sample Preparation

The following sections highlight the steps taken during the optimisation of sample preparation and the reasoning behind the final conditions chosen.

6.1.1 Diamond MPCVD 1

Previously, with one-hour growth of low-quality diamond TEC experiments were not successful. This could have been due to insufficient heat absorption by the diamond and consequently more heat reaching the collector causing thermal expansion. Figure 23 confirms this possibility, where the sharp increase of current approximately 500 seconds after temperature was first raised implies a short circuit is occurring. The collector and emitter are touching providing a direct route for electrons to cross over. For successful thermionic emission the current would have risen 10's of seconds after the temperature was first increased, not 500 seconds. Both the HB1 and HB2 samples snapped along the holes during preliminary TEC experiments, as shown in the SEM picture in Figure 24, further confirming the collector may have been pressing on them. A growth time of 2 hours was subsequently used in order to eliminate thermal expansion as the reason for unsuccessful TEC.

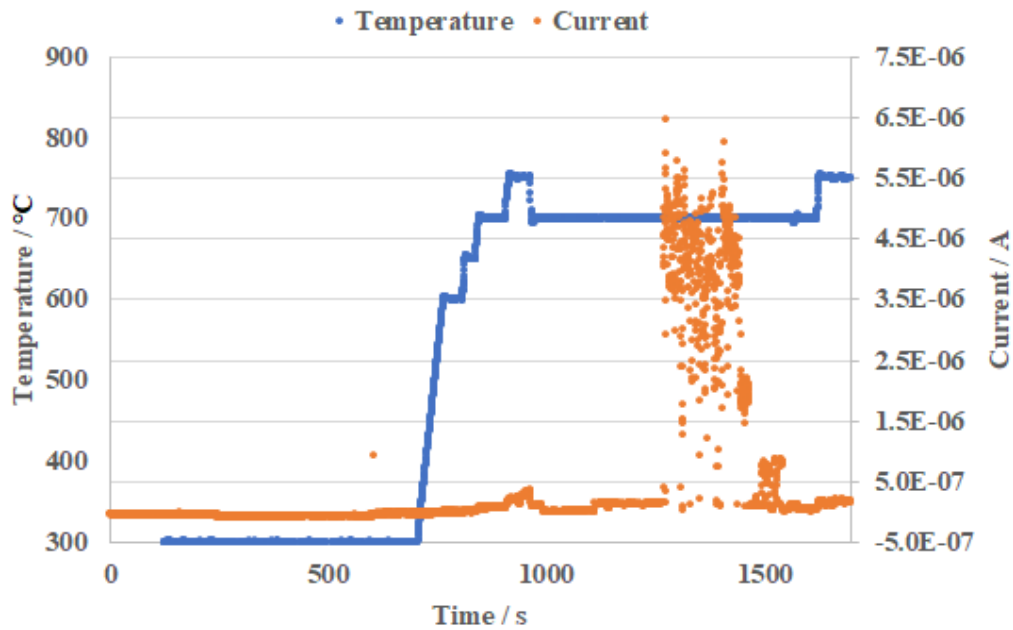


Figure 23. Graph showing how current varied with temperature during run 1 of HB1.

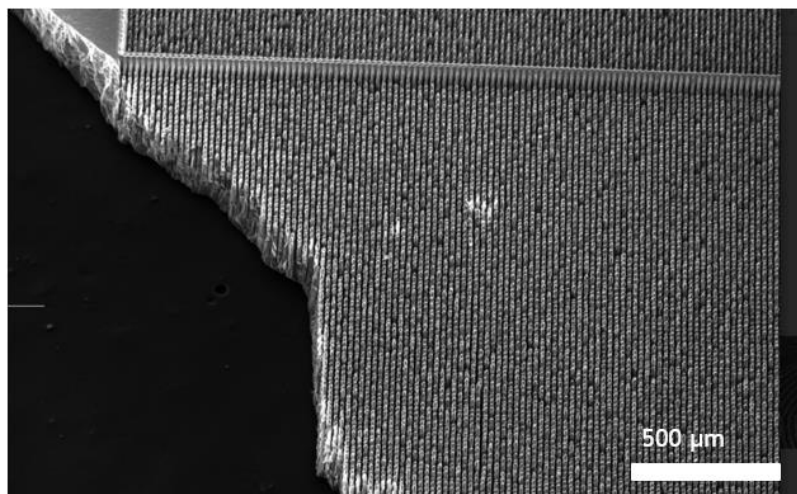


Figure 24. SEM image of HB1 showing the breakage along the milled holes following thermionic experiments.

6.1.2 Laser cutting

There is a competition between having as high surface area of holes as possible and the structural integrity of the sample. On the one hand, as large as area as possible of holes would be beneficial as the beta electrons from the $3 \times 3 \text{ mm } ^{63}\text{Ni}$ source below will emit randomly in all directions and a greater coverage and size of holes would capture a higher number of beta electrons. On the other hand, total time taken to drill the holes as well as the

structural integrity of the sample also had to be evaluated, especially considering the sample breaks observed with HB1 and HB2. Following optimisation, a 0.03 mm spacing and a drill time of 0.1 s for diamond and 0.075 s for molybdenum allowed the samples to undergo thermionic emission experiments without being damaged. The total time to mill both corners was also feasible - totalling approximately 33 hours for the diamond sample and 10 hours for the molybdenum.

Figure 25 displays a magnified image of a single milled hole from the back side (direction of milling). On this side, the hole is approximately 20 μm in diameter leading to a 35% coverage of holes within the 3 \times 3.5 mm array. Consideration of the whole 10 \times 10 mm sample gives a 7% coverage. Figure 26a shows the frontside of the sample after half an hour of growth. Prior to growth the holes were still smaller than on the backside, yielding beta exposure to the good quality diamond being anywhere from 0 - 7% for the sample. Previous work with the beta source incorporated into the anode had beta exposure of roughly 50%⁶⁹. In the future, in order to achieve the higher percentages of beta exposure in this set-up it would be beneficial to block emission from the sample exposing only the two 3 x 3.5 mm corners. This would provide an increased beta exposure of between 0 – 35%.

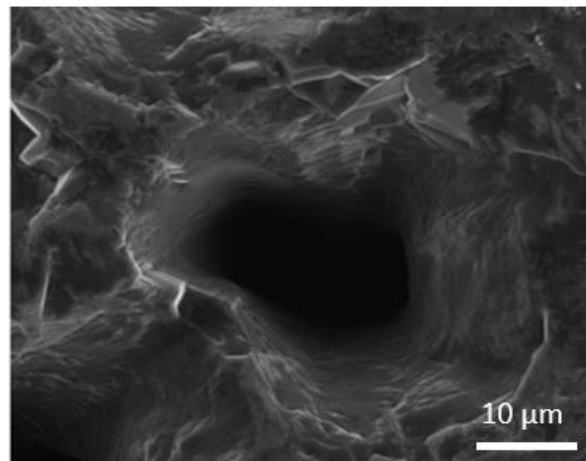


Figure 25. Close-up SEM image of a hole on HB1 from the direction of milling.

6.1.3 Final Growth

SEM images were taken to explore the extent of lateral growth in the final step. Figure 26 shows the diamond sample after half an hour of growth compared to after an hour of growth. For both samples it was necessary for the holes to be nearly completely covered in order to increase the contact of beta electrons reaching the surface of emitting diamond. To

generate a smooth lateral growth in order to avoid the growth of non-epitaxial crystals and hillocks, a methane concentration to hydrogen of less than 0.05% is required during MPCVD⁷⁴. In this report a methane to hydrogen ratio of 0.0417:1 was used, satisfying the requirement for smooth growth over the holes.

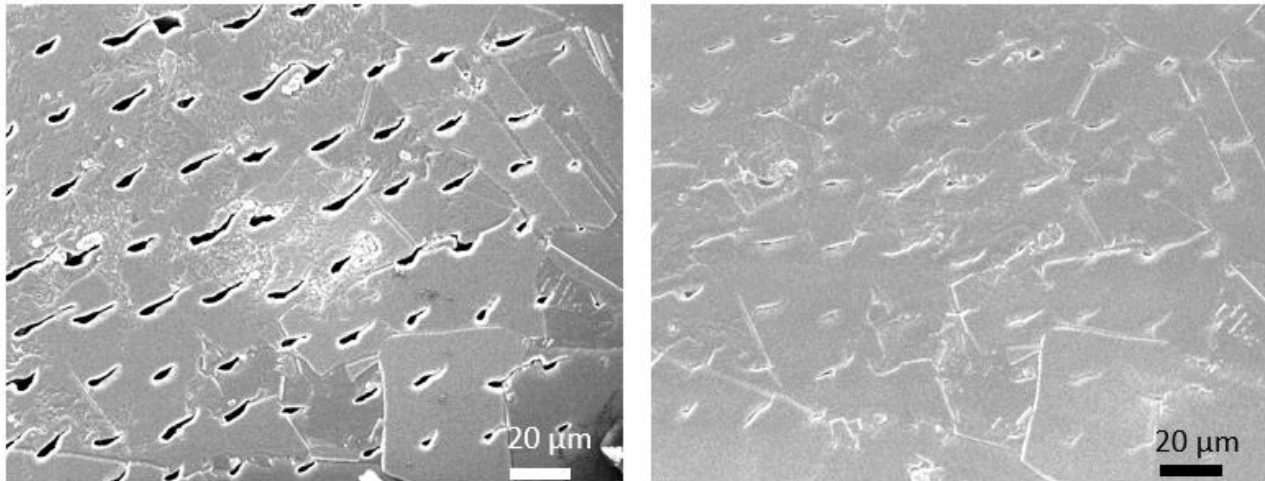


Figure 26a. (left) SEM image on the opposite side to milling after half an hour of good quality diamond growth.

Figure 26b. (right) SEM image of same area after one hour of growth.

6.1.4 H Termination

In previous studies, a run consisting of 20 profiles in which thermionic emission was measured without re-hydrogen termination was investigated. The data showed a significant drop in peak current after the first profile as the weakly bounded species were desorbed. The continued profiles showed an increase in work function as well as the threshold temperature for observed emission, as the density of low work function sites across the sample decreases with increasing desorption of hydrogen⁶⁹.

Therefore, in this report each run consists of a single profile where the sample was re-hydrogen terminated before each run. This was done in order to measure the maximum current possible as well as to solely study the effects of beta enhancement thermionic emission rather than hydrogen desorption. The importance of re-hydrogen termination was also highlighted in this report when the DC reactor was used instead of the microwave reactor and thermionic emission ceased due to ineffective termination.

6.2 Morphology Investigations

SEM was used during sample preparation to view the size and appearance of the milled holes as well as the coverage of high-quality diamond growth.

6.2.1 HMo1

It is interesting to note the SEM images for the molybdenum sample. Both $\{100\}$ and $\{111\}$ facets can be observed in the no hole corner and middle of the sample respectively. There is cauliflower like growth around the holes as shown in Figures 27c and 27d. The morphologies differ in that the $\{100\}$ diamond has two dangling bonds present on the surface and appears cubic whereas the $\{111\}$ has one dangling bond present and appears triangular.

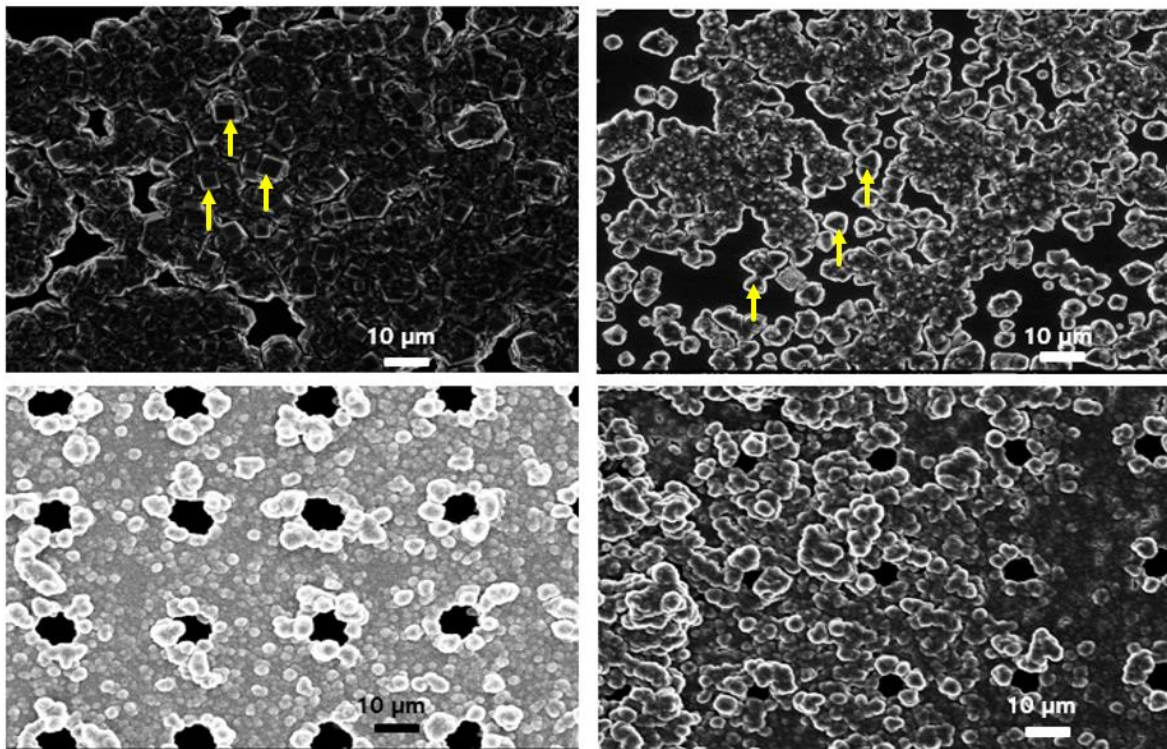


Figure 27. SEM images for the molybdenum sample **a.** (top left) $\{100\}$ cubic facets present in the no hole corner. **b.** (top right) $\{111\}$ triangular facets present in the middle of the sample. **c & d.** (bottom left & right) Cauliflower like growth in the two milled hole corners. The yellow arrows indicate examples of the cubic and triangular facets.

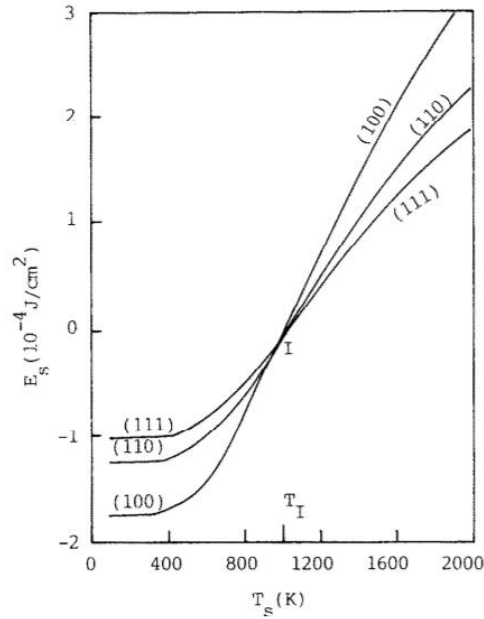


Figure 28. Growth surface energies of CVD diamond (E_s) with respect to the temperature of the substrate (T_s)⁷⁵.

Diamond growth occurred at approximately 1173 K, close to T_I on Figure 28. When the substrate temperature is below T_I , the {100} facets have the lowest surface energy and therefore are the most stable structure. It was noted that the molybdenum sample was slightly bent during growth, and the two corners where the holes were milled appeared at a higher temperature. There is a large amount of nucleation around the holes possibly due to the higher temperature and the increased surface roughness. The corners with no holes could have possibly been at a lower temperature than T_I , which produces the more stable {100} facets. The middle of the sample could have been at a temperature above T_I but below the temperature of the milled corners, producing the more stable {111} facets. Due to the superior mechanical properties of the {100} diamond it would possibly be advantageous to aim for this growth when considering the design of a diamond battery.

The valence of 3 in Boron allows easy incorporation into the {111} facets during diamond doping. This is not observed with {100} diamond leading to a reduction in electrical conductivity by a factor of 10^4 in comparison to {111}⁷⁶. When considering *p*-type Schottky diodes for energy harvesting it would be wise to consider the conductivity advantages of growing {111} diamond in order to achieve high levels of *p*-type doping.

6.3 Thermionic Emission

6.3.1 Thermionic experiments

Due to technical difficulties beta enhancement was only investigated with the diamond HB4 sample. HB4 underwent 13 runs using the MPCVD for hydrogen termination, totalling 6 runs with the presence of ^{63}Ni and 7 runs without. Figure 29 displays the variance of current with temperature for a typical run. The increase in current for the diamond sample is on the micro scale which is extremely small for practical use. Initial experiments prompted the preparation of a more conductive molybdenum sample with the aim of reaching higher peak current production. Whilst on the micro scale, current production is still useful for the comparison with and without beta exposure.

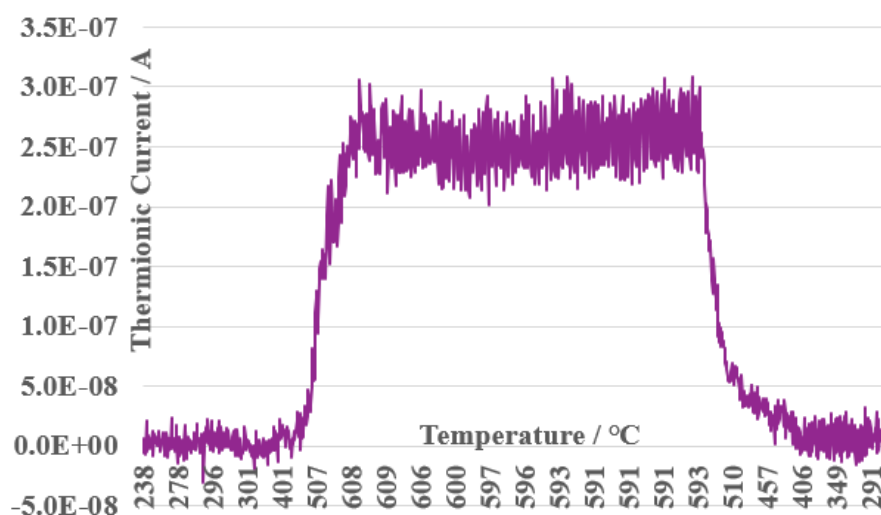


Figure 29. Graph to show typical behaviour of thermionic current with temperature.

6.3.2 Beta Enhanced Thermionic Emission (BETE)

For each run the peak current was measured and plotted as shown in Figure 30. In previous studies, the first two points have always been extremely high in comparison and can therefore be ignored for calculation. Run 13 also breaks from the trend producing a greater peak current in comparison to runs 3 - 12. Following inspection of the TEC set up it became apparent the sample stage was slightly bent which would have tilted part of the sample towards the collector, reducing the interelectrode gap and increasing emission. Therefore, run 13 was also omitted from calculations. With each hydrogen termination the high energy electron plasma may cause slight alterations on the surface. Therefore, each run was treated as its own experiment so there are no error bars.

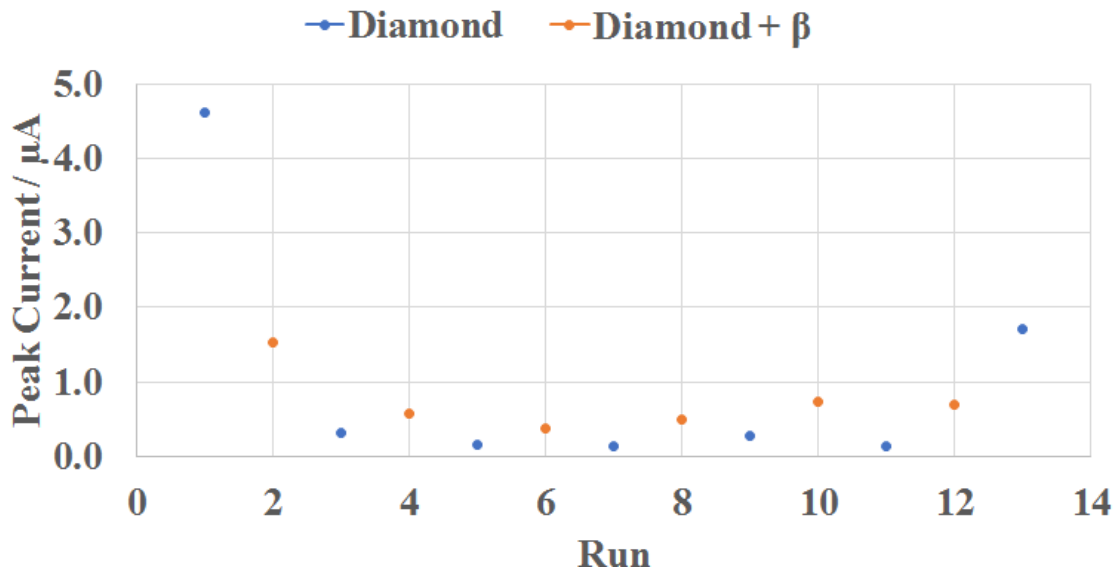


Figure 30. Graph displaying peak current against the run number. The blue dots represent the set up without inclusion of ^{63}Ni and the orange dots represent with the inclusion of ^{63}Ni . Runs 1, 2 and 13 have been omitted for calculations.

From runs 3 – 12 there is a clear increase in peak current produced with the presence of beta electrons. The average peak current for ^{63}Ni runs was $5.75\text{E-}07 \pm 2.05\text{E-}07$ A, whilst the average without ^{63}Ni was $2.01\text{E-}07 \pm 8.72\text{E-}08$ A. The averages do not overlap even with the inclusion of error and so BETE can be confirmed. Overall, from the average peak current values there is 65% beta enhancement. Previous work with the ^{63}Ni incorporated into the anode gave beta enhancement in excess of 100% each time. However previously beta exposure was just over 50%, in this case the maximum possible exposure was 7% so percentage enhancement cannot be directly compared.

6.3.3 Mechanism of BETE

There are three likely explanations for the mechanism behind beta enhanced thermionic emission.

1) SEE

SEE is the emission of surface and subsurface electrons from the sample following an interaction and transfer of energy from an incoming beta electron. Secondary electron yield is defined as the following equation, where i_s is the current of all electrons leaving the surface, and i_p is the primary current of the incoming electrons ⁷⁷.

$$\delta = \frac{i_s}{i_p} \quad (5)$$

Assuming maximum beta exposure to the emitting diamond surface of 7% with 100% successful entrance and interaction with the charge carriers in the emitter, there are approximately 1.9 million incoming primary electrons per second from the 2.6 MBq ^{63}Ni . Even with a generous secondary electron yield of 100, the secondary current would be approximately 6 pA ⁶⁸. This value is five times of order magnitude below the lowest current outputs in this report, even with the maximum 7% exposure. Therefore, although SEE is likely to occur it is not the main explanation for BETE.

2) RIC

Nitrogen doped diamond has a deep donor level sitting at 1.7 eV below the conduction band and, the consequent low concentration of charge carriers present results in a low conductivity at room temperature. This is highlighted by Figure 31 which plots the log of the carrier concentration against the inverse temperature for a *n*-type semiconductor. At low temperatures in the extrinsic region (A) there are very few electrons in the conduction band. As temperature starts to rise more electrons are donated into the conduction band until the donor orbitals are depleted – resulting in the exhaustion region (B). When temperatures are high enough electrons are donated from the valence band to the conduction band, in the intrinsic region (C). The donated electrons from the valence band in C are much greater in number than the donated electrons from the donor orbitals in A and doping effects become less important at high temperatures.

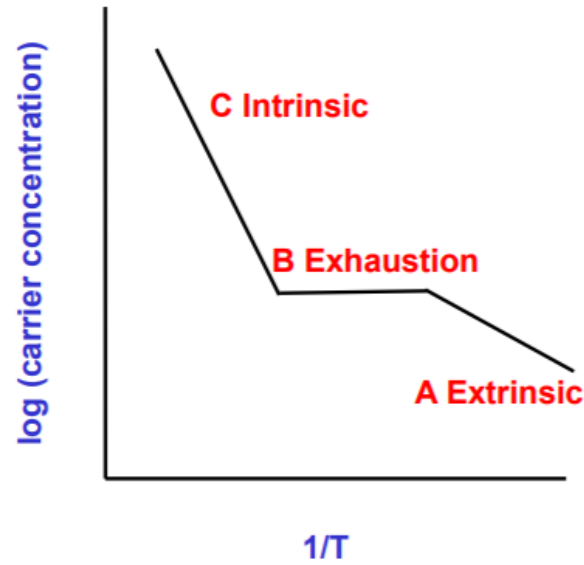


Figure 31. Graph to show the variance of conductivity with temperature for a typical semiconductor.⁷⁸

Another explanation for BETE could come from high energy beta particles creating electron hole pairs and further increasing the concentration of charge carriers in the sample. The relationship of the line shown in Figure 31 would be the same under beta irradiation however the line would be situated higher to cater for the increased concentration of charge carriers. A greater number of charge carriers will increase the conductivity and thermionic current output of nitrogen doped diamond as more electrons are able to move towards the surface to be emitted.

Previous work at Bristol has studied this mechanism in detail in order to confirm its role in BETE. Croot et al prepared a diamond thin film on an insulating diamond substrate and the resistance of the film was measured at 300°C and at 600°C with and without beta irradiation. No change of resistance was observed due to the insulating diamond preventing the motion of charge carriers⁶⁸. Further confirmation comes from working out the number of electron-hole pairs created from each beta electron using an approximate equation.

$$\phi_{EHP} = \frac{E_{\beta}}{2.5 \times E_g} \quad (6)$$

Where ϕ_{EHP} is the yield of electron-hole pair production, E_{β} is the energy of the incoming beta particle and E_g is the band gap of diamond⁶⁹. Using an average beta energy of 17.3 KeV would suggest a production of approximately 1300 electron-hole pairs per beta

electron at any given time. The significant increase in charge carrier concentration would predict a higher conductivity and consequently a greater thermionic emission upon beta irradiation.

3) Skewing of conduction band electron distribution

Another potential mechanism considers a boost in thermionic emission that is not caused by a change in conductivity. Upon interaction, the beta particles disrupt conduction band electrons from their equilibrium into higher energy states. These electrons would be considered to emit easily however due to the upward band bending they become trapped. When heated during the TEC these electrons are able to emit adding another component to the thermionic emission ⁶⁸.

Garret et al presented a study introducing a kappa component into the Richardson – Dushman equation in order to cater for this effect. Which shows at low values of κ , emission can increase between four and five orders of magnitude with respect to the classical Richardson – Dushman equation. This large increase in emission at lower temperatures would not bode well for the efficiency of thermionic converters due to the requirement of a high temperature emitter. Further research would need to look at the emission of a sample at different temperatures in order to decipher whether the trend switches to follow the kappa Richardson – Dushman or the classical equation upon irradiation with beta particles ⁷⁹.

6.3.4 Threshold temperature

The correlation between threshold temperature and beta was also investigated, where the threshold temperature was taken to be the temperature at which the current first begins to rise. As shown by Figure 32 there does not appear to be a trend between threshold temperature and peak current. Threshold temperature was investigated as it would show a more efficient device if emission was observed at lower temperatures.

In contrast, the y – axis shows a relationship between peak current and the presence of beta electrons as previously discussed. It is interesting to note that the beta electrons only appear to cause enhancement once thermionic emission is already taking place. This could act as evidence to the third mechanism playing the main part during beta enhancement, whereby, a minimum energy input is required for the emission of the skewed conduction band electrons. If radiation induced conductivity was taking place, there might be an expected

increase of thermionic emission at lower temperatures due to the production of 1300 electron hole pairs per beta electron regardless of temperature.

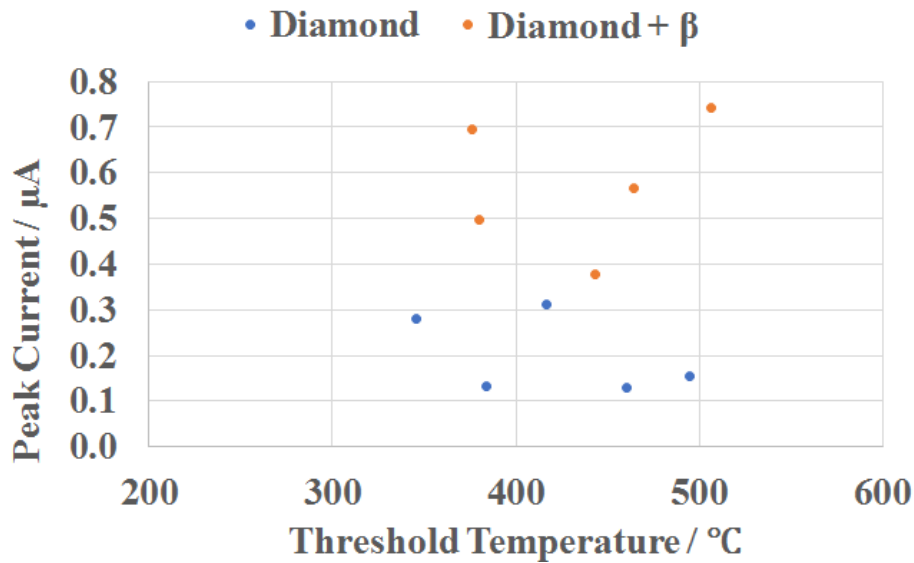


Figure 32. Graph to show peak current against threshold temperature for runs 3 - 12.

Figure 33 shows the threshold temperature over the series of runs. Aside from run 10, there appears to be a general decrease in threshold temperature with each experiment. This graph suggests that with each termination the sample is producing thermionic emission more readily. One possibility is that from repeated cycles of heating and termination are producing a higher density of low work function sites across the sample that alter the threshold temperature but not the peak current.

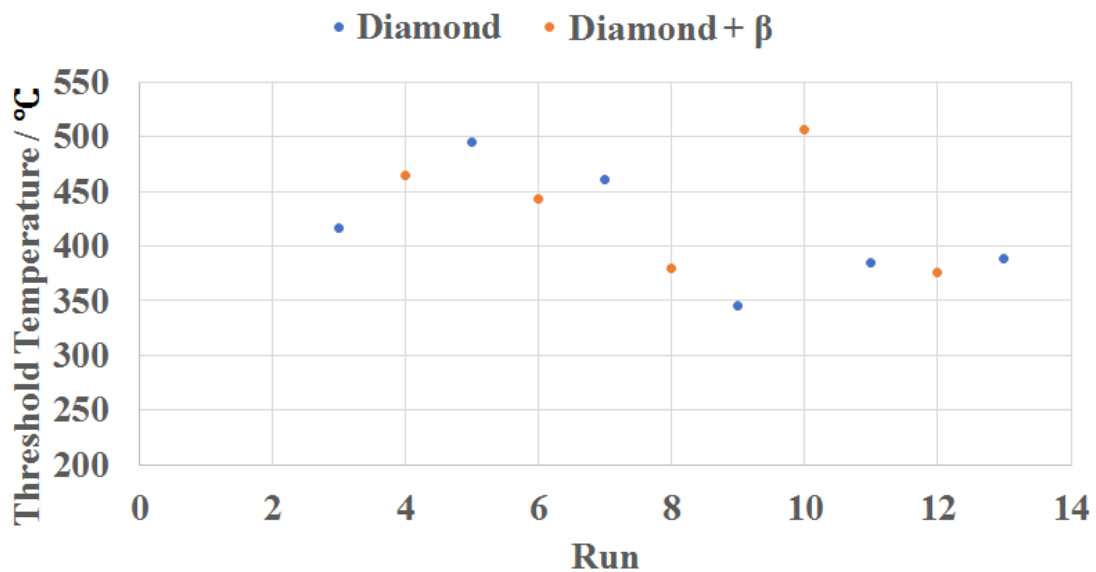


Figure 33. Graph to show threshold temperature against run number, if run 10 is treated as an anomaly there appears to be a decrease in temperature with increasing runs.

6.3.5 Further observations

The following graphs represent the relationship between current and temperature over time for earlier runs compared to later runs. The later runs show the expected relationship for a hydrogen terminated semiconductor, where at 600°C the hydrogen desorbs raising the work function of the surface; this in turn causes a drop in thermionic current before the temperature is lowered. However, the first five runs showed the trend seen in Figure 34. In this case, the thermionic current appears to keep rising whilst the temperature remains at 600°C. This could possibly be due to the sample being fresh from growth for the earlier runs and there being a contribution to current from hydrogen releasing from the bulk. With repeated terminations and cycling of heat this bulk hydrogen is eventually depleted and for later runs the only hydrogen is that on the surface.

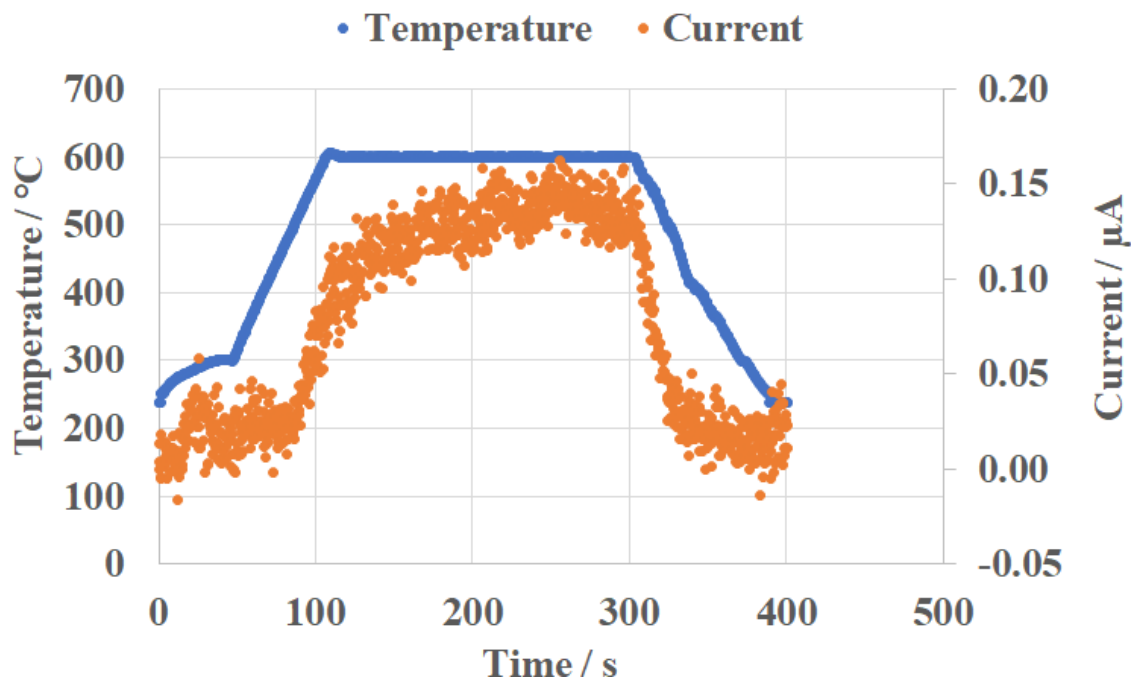


Figure 34. Graph to show how current varied with temperature over time. This graph is run 5 (no beta exposure) and represents the relationship seen for the first 5 runs.

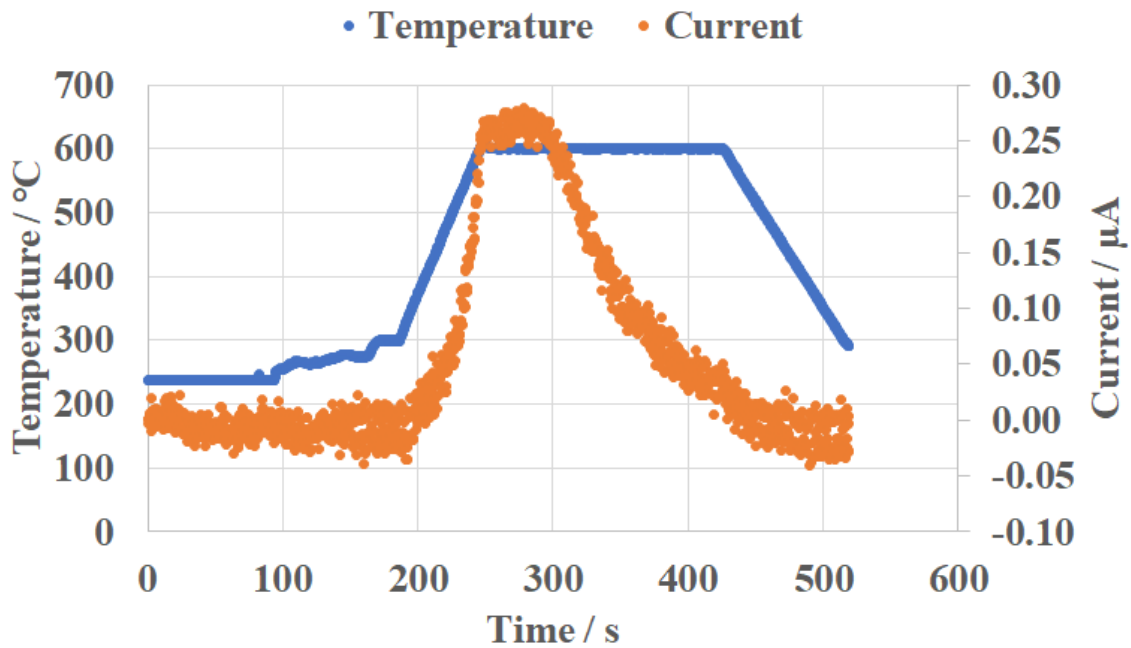


Figure 35. Graph to show how current varied with temperature over time for the later runs. This graph is run 9 (no beta exposure).

6.4 Deuterium Terminations

Deuterium terminations were investigated on both samples in order to see any effect the heavier isotope of hydrogen might have on thermionic emission. All D-terminations were carried out in closed cycle conditions. A report by Guenette et al has looked at exposing diamond to D plasmas, whereby they found the D plasma caused surface erosion which was redeposited as graphitic carbon⁸⁰. Deuterium surfaces are expected to produce the same NEA surfaces as hydrogen and so prior to experiments it could possibly be expected that D terminations would increase thermionic emission due to the enhanced conductivity⁸¹.

Figure 36 shows peak current against the sample type, the termination and the conditions of the MPCVD cycle. The H-terminated more conductive molybdenum sample shows higher peak emission than the diamond sample as expected. D-terminated molybdenum showed approximately half the emission to flowing H-terminated molybdenum. In order to determine whether the lower emission observed was due to the deuterium or closed cycle conditions, H-terminated closed cycle molybdenum was tested which showed zero emission. The same experiments were carried out with HB4, however in this case the D-

terminated sample showed slightly higher emission and the closed cycle H-termination gave the same emission as flowing hydrogen.

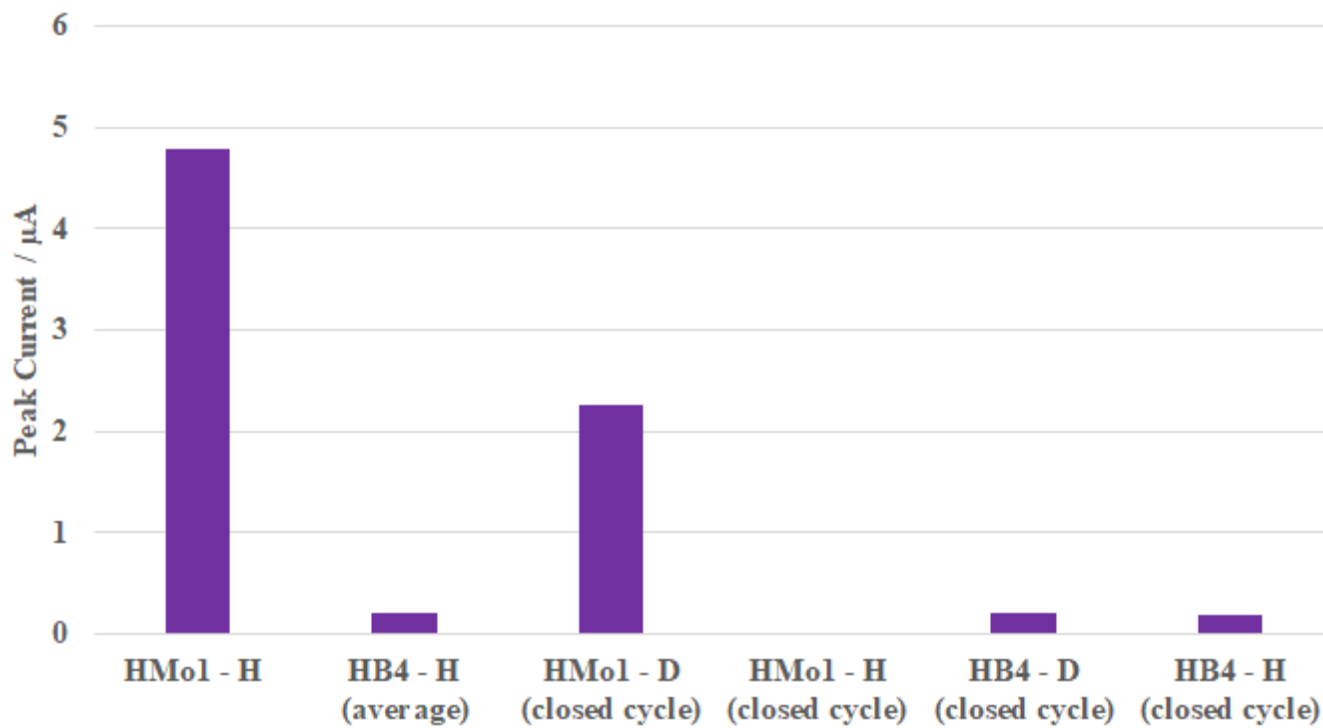


Figure 36. Bar graph to show the peak current reached under the different samples, terminations, and free flowing or closed cycle conditions.

The results shown here are preliminary and more experiments would have to be carried out to give conclusive evidence on the behaviour of deuterium terminations on emission. During the ‘cleaning’ step off termination molecules such as oxygen will be removed from the surface, however, in closed cycle conditions these molecules will not be vented away and could possibly be re-adsorbing on the surface. A study by Michaelson et al showed deuterium surfaces are more likely to be contaminated at ambient conditions due to the higher sp^2 nature present⁸². In the case of molybdenum, this could explain the lower observed emission however it does not appear to have affected the HB4 sample and the effects may only become obvious at higher emissions.

Another interesting observation occurred after the D-terminated HB4 underwent another emission test without re-termination, whereby, peak current reached the same value as before. The same test was repeated with H-terminated HB4, however this time there was no emission. Deuterium is heavier than hydrogen resulting in the vibrational frequency of the

C-D bond being a lot lower than the C-H bond. Therefore, the strength of the C-D bond is approximately 3 kJ mol^{-1} higher than that of C-H⁸³. Deuterium at 600°C does not appear to desorb, this is not the case for C-H where the hydrogen desorbs and the current falls straight away. Deuterium is expected to desorb at temperatures greater than 1250°C , which is advantageous for devices to undergo repeated emissions at temperatures below this⁸¹.

7 Future Outlooks

1) Beta enhancement

Firstly, to directly compare integration of the beta source into the cathode over the anode a higher beta exposure would have to be accomplished. Using the same experimental set-up, this could be achieved by cutting the appropriate shape out of silicon to place over the diamond leaving only the array of holes exposed. Looking into the future, it would be beneficial to have the beta electrons incorporated into the lattice of the emitter. Diamond is still an excellent candidate for this proposal as it can be grown using C^{14} which emits beta electrons. C^{14} has a half-life of 5730 years and the average beta energy 49 keV^{84 85}. The higher beta energy would predict a greater number of electron hole pairs produced according to equation 6 in section 6.3.2, as well as a greater skewing of electron energy states satisfying both possible mechanisms. The ^{14}C properties coupled with the greater beta exposure predict a much larger increase in beta enhancement. For the long term, there is an abundance of ^{14}C in the UK lying around as radioactive waste. However, for lab use ^{13}C can be used during growth to mitigate radioactive waste handling. ^{13}C is able to be transmuted into ^{14}C when bombarded with neutrons.

The output current is extremely low for the diamond sample; therefore, it would be beneficial to test the more conductive molybdenum sample for beta enhancement to see if there are any dramatic differences with conductivity. Greater conductivity could possibly be achieved using the diamond sample by etching the surface. This would produce graphitic carbon along the etches adding to the conductive networks.

2) Deuterium enhancement

Following on from these deuterium investigations, a larger number of runs would need to be carried out for each of those shown in Figure 36. The purpose of this is to

conclude for certain how deuterium termination affects the emission of HMo1 and HB4 and also to determine if the closed cycle or the nature of the termination changes the emission more. The more stable C-D bond has potential and it would be interesting to test multiple runs at higher temperatures. According to the Richardson – Dushman equation thermionic current is proportional to the square of the temperature and so it would be advantageous to see the possible peak current outputs at higher temperatures. Runs should also be performed without re-termination to see how long D resists thermal desorption. For practical purpose it is advantageous for a thermionic device to repeatedly produce a high current without having to do repeated terminations.

3) Beta & deuterium

There is potential to combine the beneficial effects of beta and deuterium by growing samples in a deuterium atmosphere during MPCVD. As with the C^{13} samples, bombardment with neutrons can turn the deuterium into tritium. Tritium has a half-life of 12 years and produces beta electrons with an average energy of 5.7 KeV ⁸⁶. Both values are lower than the beta electrons from ^{63}Ni and ^{14}C and a smaller beta enhancement can therefore be predicted. The shorter half-life would mean devices would have to be maintained and updated more frequently than the other radioisotope devices. It is important to study the benefits that deuterium can offer in order in relation to the disadvantages when considering beta enhanced thermionic devices.

8 Conclusion

Two thermionically emitting samples, HMo1 and HB4, with the ability to incorporate ^{63}Ni were successfully prepared. Beta enhancement of 65% was observed for HB4 which correlated to a beta exposure of a maximum of 7%. Although the beta exposure is lower than expected, the beta enhancement is significant and this is likely to be due to an increase in conductivity caused by the incoming radiation creating electron hole pairs. Another possible mechanism comes from the alteration of the skew of electrons with many being in higher energy states following the beta interaction. When heated by the laser these electrons may leave the conduction band and contribute to the thermionic current.

Further experiments highlighted the importance of temperature for diamond growth and successful termination. SEM images displayed how diamond morphology varied with

temperature across HMo1. Thermionic emission was not seen when terminations were attempted at lower temperatures indicating that the hydrogen induced NEA was not present. There did not appear to be a relationship between the threshold temperature and peak current, however, repeated runs on a sample appeared to lower the threshold temperature. Repeated runs on a sample could possibly induce a greater density of low work function sites which could benefit thermionic devices with the potential to start emission at lower temperatures.

Deuterium terminations proved to be effective in producing a thermionic current. Following preliminary experiments there can be no conclusive statement on the effect deuterium has on enhancement, and further work would have to be carried out. The stronger C-D bond makes for a more stable surface however, which is beneficial for thermionic emission as it allows for repeated experiments at higher temperatures without re-termination.

9 Acknowledgements

I would firstly like to thank Neil Fox for the initial project proposal and his input and motivation throughout the year to try new ideas. I am also grateful to Paul May for his advice, Ed Smith for all the help with the microwave reactor including a last-minute deuterium addition, and Amelia Billings for all the company and laughs in the diamond office. I am incredibly grateful to Gary Wan who taught me in depth about everything I used in the diamond lab and for making this year a really enjoyable experience.

10 References

- 1 R. H. Pratt, A. Ron and H. K. Tseng, *Rev. Mod. Phys.*, (1973), **45**, 273–325.
- 2 G. P. Smestad, *Sol. Energy Mater. Sol. Cells*, (2004), **82**, 227–240.
- 3 J. Szymanski, A. J. Butterfield, *A Dictionary of Electronics and Electrical Engineering (5 ed.)*, Oxford University Press, (2018).
- 4 S. Liang, L. K. Ang and G. Chen, *PIERS Proc.*, (2014), 906–908.
- 5 D. B. Go, J. R. Haase, J. George, J. Mannhart, R. Wanke, A. Nojeh and R. Nemanich, *Front. Mech. Eng.*, (2017), **3**, 1–17.
- 6 V. C. Wilson, *J. Appl. Phys.*, (1959), **30**, 475–481.
- 7 F. L. Curzon and B. Ahlborn, *Am. J. Phys.*, (1975), **43**, 22–24.
- 8 Q. Le, Y. Chen, X. Wang, Y. Li, J. Hong and J. Xu, *Investig. Ophthalmol. Vis. Sci.*, (2011), **52**, 8951–8956.

- 9 O. H. K. Reck, F. Dionigi, *Photon-Enhanced Thermionic Emission in Cesium-doped p-Type and n-Type Silicon*, WIP, (2014).
- 10 Z. Li, B. Bai, C. Li and Q. Dai, *Carbon N. Y.*, (2016), **96**, 641–646.
- 11 J. R. Smith, *J. Appl. Phys.*, (2013), **114**, 1–16.
- 12 F. A. M. Koeck, R. J. Nemanich, Y. Balasubramaniam, K. Haenen and J. Sharp, *Diam. Relat. Mater.*, (2011), **20**, 1229–1233.
- 13 S. Meir, C. Stephanos, T. H. Geballe and J. Mannhart, *J. Renew. Sustain. Energy.*, (2013), **5**, 043127.
- 14 I. Bickerton and N. A. Fox, *Front. Mech. Eng.*, (2017), **3**, 1–4.
- 15 E. Erlich and D. Hausel, in *Diamond Deposits*, SME, Littleton, (2002), p.5.
- 16 Y. Takano, *J. Phys. Condens. Matter.*, (2009), **21**, 253201.
- 17 J. Philip, P. Hess, T. Feygelson, J. E. Butler, S. Chattopadhyay, K. H. Chen and L. C. Chen, *J. Appl. Phys.*, (2003), **93**, 2164–2171.
- 18 A. R. Oganov, R. J. Hemley, R. M. Hazen and A. P. Jones, *Rev. Mineral. Geochemistry*, (2013), **75**, 47–77.
- 19 C. M. Sung and M. F. Tai, *Int. J. Refract. Met. Hard Mater.*, (1997), **15**, 237–256.
- 20 R. A. Khmel'nitsky and A. A. Gippius, *Phase Transitions*, (2014), **87**, 175–192.
- 21 Y. Chen, L. C. Zhang, in *Polishing of Diamond Materials*, Springer, (2013), ch. 2, pp. 14.
- 22 P. T. Moseley, D. A. J. Rand and K. Peters, *J. Power Sources*, (2015), **295**, 268–274.
- 23 K. E. Spear and J. P. Dismukes, *Synthetic Diamond: Emerging CVD Science and Technology*, Wiley, (1994).
- 24 Diamond and graphite properties, <http://phycomp.technion.ac.il/~david/thesis/node3.html>.
- 25 R. Abbaschian, H. Zhu and C. Clarke, *Diam. Relat. Mater.*, (2005), **14**, 1916–1919.
- 26 R. M. Nor R.M., Bakar S.A., Thandavan T.M., in *Carbon and Oxide Nanostructures*, Springer, Berlin, Heidelberg, Berlin, (2010), vol. 5, pp. 23–49.
- 27 and S. K. T. Yamamoto, S. D. Janssens, R. Ohtani, D. Takeuchi, *Appl. Phys. Lett.*, (2016), **109**, 182102.
- 28 T. A. Railkar, W. P. Kang, H. Windischmann, A. P. Malshe, H. A. Naseem, J. L. Davidson and W. D. Brown, *Crit. Rev. Solid State Mater. Sci.*, (2000), **25**, 163–277.
- 29 J. A. Smith, K. N. Rosser, H. Yagi, M. I. Wallace, P. W. May and M. N. R. Ashfold, *Diam. Relat. Mater.*, (2001), **10**, 370–375.
- 30 X. J. Li, S. Zhou, G. Chen, D. Sen Wang, N. Pei, H. L. Guo, F. M. Nie, X. Zhang and S. Feng, *Def. Technol.*, (2018), **14**, 373–379.
- 31 S. Kumar, M. Jadhav, R. Bajpai, D. S. Misra, K. Das Gupta and R. Varma, *Proc. DAE Symp. Nucl. Phys.* 58, (2013), **58**, 920–921.
- 32 J. E. Butler, Y. A. Mankelevich, A. Cheesman, J. Ma and M. N. R. Ashfold, *J. Phys. Condens. Matter*, (2009), **21**, 364201.
- 33 H. Liu and D. S. Dandy, *Diam. Relat. Mater.*, (1995), **4**, 1173–1188.
- 34 P. A. Nistor and P. W. May, *J. R. Soc. Interface*, (2017), **14**, 20170382.

- 35 D. M. Gruen, *Annu. Rev. Mater. Sci.*, (1999), **29**, 211–259.
- 36 P. W. May, *Phil. Trans. R. Soc. Lond. A*, (2000), **358**, 473–495.
- 37 J. E. Butler and A. V. Sumant, *Chem. Vap. Depos.*, (2008), **14**, 145–160.
- 38 M. H. Nazare and A. J. Neves, *properties, growth and applications of diamond*, INSPEC, HERTS, (2001).
- 39 P. Hess, *J. Appl. Phys.*, (2012), **111**, 051101.
- 40 D. Joag, M. More and F. Jamali Sheini, in *Nanowires - Implementations and Applications*, ed. H. Abbass, InTech, (2011), p. 526.
- 41 R. Harniman, P. W. May and O. J. L. Fox, *Diam. Relat. Mater.*, (2017), **80**, 147–152.
- 42 V. Mortet, O. Elmazria, M. Nesladek, M. B. Assouar, G. Vanhoyland, J. D’Haen, M. D’Olieslaeger and P. Alnot, *Appl. Phys. Lett.*, (2002), **81**, 1720.
- 43 C. J. H. Wort and R. S. Balmer, *Mater. Today*, (2008), **11**, 22–28.
- 44 B. Cordero, V. Gómez, A. E. Platero-Prats, M. Revés, J. Echeverría, E. Cremades, F. Barragán and S. Alvarez, *J. Chem. Soc. Dalt. Trans.*, (2008), 2832–2838.
- 45 L. Diederich, O. M. Küttel, E. Schaller and L. Schlapbach, *Surf. Sci.*, (1996), **349**, 176–184.
- 46 Z. Zhang and J. T. Yates, *Chem. Rev.*, (2012), **112**, 5520–5551.
- 47 M. T. Edmonds, C. I. Pakes, S. Mammadov, W. Zhang, A. Tadich, J. Ristein and L. Ley, *Phys. Status Solidi Appl. Mater. Sci.*, (2011), **208**, 2062–2066.
- 48 P. Hubik and J. Mares, in *Thermal Analysis of Micro, Nano, and Non-crystalline Materials*, eds. J. Sestak and P. Simon, Springer, Berlin, Heidelberg, New York, London, (2013), p. 377.
- 49 W. Chen, D. Qi, X. Gao and A. T. S. Wee, *Prog. Surf. Sci.*, (2009), **84**, 279–321.
- 50 J. B. Cui, J. Ristein and L. Ley, *Phys. Rev. Lett.*, (1998), **81**, 429–432.
- 51 P. Aebi, L. Schlapbach, O. M. Küttel and L. Diederich, *Surf. Sci.*, (1998), **418**, 219–239.
- 52 W. F. Paxton, S. Ravipati, M. M. Brooks, M. Howell and J. L. Davidson, *Front. Mech. Eng.*, (2017), **3**, 18.
- 53 A. K. Tiwari, J. P. Goss, P. R. Briddon, A. B. Horsfall, N. G. Wright, R. Jones and M. J. Rayson, *Epl*, (2014), **108**, 0–6.
- 54 C. R. Valenta, M. M. Morys and G. D. Durgin, *IEEE Trans. Microw. Theory Tech.*, (2015), **63**, 1758–1767.
- 55 C. R. Valenta, in *2015 IEEE International Conference on RFID Technology and Applications (RFID-TA)*, IEEE, (2015).
- 56 J. Goldstein, D. Newbury, J. Michael, N. Ritchie, J. Scott and D. Joy, *Scanning Electron Microscopy and X-Ray Microanalysis*, Springer Nature, USA, (2018).
- 57 G. Wickham and D. Worthen, *Int. Ophthalmol. Clin.*, (1973), **13**, 19–32.
- 58 Y. Gao, Y. F. Lu, J. Bai, Z. Q. Xie, T. Guillemet, J. Park, Y. S. Zhou, X. C. Zeng and L. Jiang, *Sci. Rep.*, (2014), **4**, 1–7.
- 59 J. Wilks and E. Wilks, *Properties and Applications of Diamond*, Butterworth-Heinemann, Oxford, (1992).
- 60 I. V. Kovalev, V. G. Sidorov, P. V. Zelenkov, A. Y. Khoroshko and A. T. Lelekov, *IOP Conf.*

- Ser. Mater. Sci. Eng.*, (2015), **94**, 012024.
- 61 Y. R. Uhm, B. G. Choi, J. B. Kim, D. H. Jeong and K. J. Son, *Nucl. Eng. Technol.*, (2016), **48**, 773–777.
- 63 J. Yang and T. Caillat, *MRS Bull.*, (2006), **31**, 224–229.
- 64 Y. S. Nagornov and V. N. Murashev, *Semiconductors*, (2016), **50**, 17–22.
- 65 A. Horvath and E. Rachlew, *Ambio*, (2016), **45**, 38–49.
- 66 New Scientist, <https://www.newscientist.com/article/dn2951-radioactive-battery-provides-decades-of-power/>, (accessed November 2018).
- 67 University of Bristol, <http://www.bris.ac.uk/news/2016/november/diamond-power.html>, (Accessed December 2018)
- 68 A. Croot, G. Wan, A. Rowan, H. D. Andrade, J. A. Smith and N. A. Fox, *Front. Mech. Eng.*, (2017), **3**, 1–8.
- 69 A. Rowan, Thesis, University of Bristol, (2017).
- 70 Y. M. Liu, J. Bin Lu, X. Y. Li, X. Xu, R. He, R. Z. Zheng and G. D. Wei, *Chinese Phys. Lett.*, (2018), **35**, 5–9.
- 71 V. V. G. L.A. Tsvetkov, A.A. Pustovalov and V. Y. B. and A. V. Tikhomirov, in *5th International Conference on Isotopes*, (2005), p. 99.
- 72 D. T. Morelli, T. M. Hartnett and C. J. Robinson, *Appl. Phys. Lett.*, (1991), **59**, 2112–2114.
- 73 D. Horinek, A. Serr, M. Geisler, T. Pirzer, U. Slotta, S. Q. Lud, J. A. Garrido, T. Scheibel, T. Hugel and R. R. Netz, *Proc. Natl. Acad. Sci.*, (2008), **105**, 2842–2847.
- 74 T. Teraji, S. Mitani, C. Wang and T. Ito, *J. Cryst. Growth*, (2002), **235**, 287–292.
- 75 N. Lee and A. Badzian, *Diam. Relat. Mater.*, (2002), **6**, 130–145.
- 76 B. V. Spitsyn, L. L. Bouilov and B. V. Derjaguin, *J. Cryst. Growth*, (1981), **52**, 219–226.
- 77 J. J. Scholtz, D. Dijkkamp and R. W. A. Schmitz, *Philips J. Res.*, (1996), **50**, 375–389.
- 78 N. Allan, lecture, (2019).
- 79 J. L. Domenech-Garret, S. P. Tierno and L. Conde, *Eur. Phys. J. B*, (2013), **86**, 2–5.
- 80 C. S. Corr, L. Thomsen, D. P. Riley, A. Deslandes and M. C. Guenette, *Diam. Relat. Mater.*, (2014), **49**, 103–110.
- 81 O. A. Williams, *Nanodiamond*, Royal Society of Chemistry, (2014).
- 82 S. Michaelson, R. Akhvlediani and A. Hoffman, *Phys. Chem. Chem. Phys.*, (2011), **13**, 11471–11480.
- 83 Y. R. Luo, in *CRC Handbook of Chemistry and Physics*, ed. W. M. Haynes, CRC, 91st edn., (2010).
- 84 H. Godwin, *Nature*, (1962), **195**, 984.
- 85 G. H. Jenks and F. H. Sweeton, *Phys. Rev. Lett.*, (1952), **86**, 803.
- 86 W. L. Pillinger, J. J. Hentges and J. A. Blair, *Phys. Rev.*, (1961), **121**, 203.